

RESEARCH ARTICLE

10.1002/2016JD026374

Key Points:

- All-sky and clear-sky sunshine duration and global radiation trends
- Comparison for the 1959–2013 period over the Italian territory
- Discussion on whether disagreements in clear-sky trends can be due to a different sensitivity to atmospheric turbidity changes

Correspondence to:

V. Manara,
veronica.manara@unimi.it

Citation:

Manara, V., M. Brunetti, M. Maugeri, A. Sanchez-Lorenzo, and M. Wild (2017), Sunshine duration and global radiation trends in Italy (1959–2013): To what extent do they agree?, *J. Geophys. Res. Atmos.*, 122, 4312–4331, doi:10.1002/2016JD026374.

Received 13 DEC 2016

Accepted 31 MAR 2017

Accepted article online 5 APR 2017

Published online 28 APR 2017

Sunshine duration and global radiation trends in Italy (1959–2013): To what extent do they agree?

V. Manara¹ , M. Brunetti² , M. Maugeri^{1,2} , A. Sanchez-Lorenzo³ , and M. Wild⁴ 

¹Department of Physics, Università degli Studi di Milano, Milan, Italy, ²Institute of Atmospheric Sciences and Climate, ISAC-CNR, Bologna, Italy, ³Instituto Pirenaico de Ecología, Consejo Superior de Investigaciones Científicas (IPE-CSIC), Zaragoza, Spain, ⁴Institute for Atmospheric and Climate Science, ETH Zürich, Zürich, Switzerland

Abstract Two Italian homogenized data sets of sunshine duration (SD) and global radiation ($E_{g\downarrow}$) relative anomalies are used to investigate to what extent these two variables agree with respect to their temporal evolution. They are compared for northern and southern Italy over the period 1959–2013. Both under all-sky and clear-sky conditions, the SD records tend to show a shorter and less intense decrease until the 1980s (“global dimming”) with respect to the $E_{g\downarrow}$ ones, while there is a better agreement in the subsequent period when both variables increase (“brightening period”). To investigate whether such behavior can be explained by a different sensitivity of SD and $E_{g\downarrow}$ to atmospheric turbidity variations, the observed clear-sky trends are compared to those estimated by a model based both on Lambert-Beer’s law and on a simple estimation of diffuse radiation. Results show that most of the differences observed in the trends of the clear-sky SD and $E_{g\downarrow}$ records can be explained considering a realistic pattern of atmospheric turbidity in the 1959–2013 period. The only exception concerns winter and autumn in northern Italy where clear-sky SD does not decrease in the dimming period as much as it would be expected on the basis of the corresponding increase in atmospheric turbidity. One reason for this discrepancy could be the influence of other variables like relative humidity. This case study highlights that changes in atmospheric turbidity have to be kept in mind when SD is used to investigate the multidecadal evolution of $E_{g\downarrow}$.

Plain Language Summary Two homogenized datasets of sunshine duration and global radiation relative anomalies over Italy are used to investigate to what extent these two variables agree under all-sky and clear-sky conditions in terms of their decadal variations. They are compared for northern and southern Italy over the 1959–2013 common period. Global radiation shows a decreasing tendency until the mid-1980s and an increasing tendency in the following period both under all-sky and clear-sky conditions. Moreover, it shows stronger tendencies than those observed for sunshine duration. So a model has been applied in order to verify if these differences can be explained with a different sensitivity to atmospheric turbidity changes. The results show that most of the differences observed in the trends of the clear-sky sunshine duration and global radiation records can be explained considering the patterns of atmospheric turbidity in the 1959–2013 period. The only exception concerns winter and autumn in northern Italy. The reasons of this discrepancy could be due both to instrumental problems and to the influence of other variables.

1. Introduction

The amount of solar energy reaching the Earth’s surface provides the energy for a variety of climate processes (e.g., evaporation, snow melting, and diurnal/seasonal cycle of surface temperature) [Hartmann *et al.*, 1986; Ohmura and Gilgen, 1993]. Therefore, its changes can have profound environmental, societal, and economic implications [Stanhill, 1983; Wild, 2009].

Global radiation (also known as surface solar radiation— $E_{g\downarrow}$) is the solar radiation received from a solid angle of 2π sr on a horizontal surface and is measured with a pyranometer [World Meteorological Organization (WMO), 2008a]. It includes radiation received directly from the solid angle of the sun’s disc (direct radiation— E), as well as the downward component of the diffuse sky radiation that has been scattered in traversing the atmosphere (diffuse radiation— $E_{d\downarrow}$).

In the last decades, the scientific community has learned that $E_{g\downarrow}$ is not constant on decadal timescales [Wild, 2009, 2016], showing a decrease called “global dimming” from the 1950s to the 1980s [Stanhill and Cohen, 2001; Stanhill, 2005] and a subsequent increase called “brightening period” since the beginning of 1980s

[Wild *et al.*, 2005; Wild, 2012]. Series starting before the 1950s display also an increase during the 1930s and 1940s, known as “early brightening” [Stanhill and Achiman, 2016].

Causes of these variations are complex and not yet completely understood, especially if studies regarding different areas are compared. Major causes are thought to be related to changes in anthropogenic aerosols and cloud characteristics [Liepert *et al.*, 1994; Stanhill and Cohen, 2001; Wild, 2009, 2016; Chiacchio and Wild, 2010; Xia, 2010; Matuszko, 2012; Bartók, 2016]. Clouds are supposed to be the major contributors to the $E_{g\downarrow}$ variability at interannual scale, while atmospheric aerosols contribute especially at decadal scale [Wang *et al.*, 2012; Wild, 2016] even if they are not completely independent [Ramanathan *et al.*, 2001; Xia, 2012].

In particular, increasing anthropogenic aerosol emissions from the 1950s are thought to be the major cause of the observed decadal $E_{g\downarrow}$ reduction until the 1980s [Stanhill and Cohen, 2001; Liepert and Tegen, 2002; Norris and Wild, 2007]. However, measures to reduce air pollution from the 1970s onward have been suggested to be responsible for the renewed increase of $E_{g\downarrow}$ [Hansen *et al.*, 1997; Dutton *et al.*, 2004, 2006; Vestreng *et al.*, 2007; Chiacchio and Wild, 2010; Nabat *et al.*, 2014]. The reasons for the observed increase during the 1930s and 1940s are more difficult to determine, considering the low availability of long records [Wild *et al.*, 2009; Antón *et al.*, 2014, 2017; Sanchez-Lorenzo *et al.*, 2015; Wild, 2016].

$E_{g\downarrow}$ records started to become available on a widespread basis only in the late 1950s [Stanhill, 1983; Wild *et al.*, 2009]. Consequently, one of the main problems in studying the temporal variability of $E_{g\downarrow}$ is the small number of sites with reliable long-term records. Therefore, proxy measures available for longer periods such as total cloud cover (TCC), visibility, and sunshine duration (SD) [Stanhill, 2005; Sanchez-Lorenzo *et al.*, 2009; Wang *et al.*, 2012; Román *et al.*, 2014; Antón *et al.*, 2017] are helpful to estimate the temporal variability of $E_{g\downarrow}$. The most appropriate proxy for $E_{g\downarrow}$ is probably SD because it is less subjective than the others and data are available since the late nineteenth century [Sanchez-Lorenzo *et al.*, 2013]. Moreover, SD is closely correlated to $E_{g\downarrow}$ by means of the Ångström-Prescott formula [Ångström, 1924; Prescott, 1940].

According to the WMO, the SD for a given day is the length of time during which E is above 120 W m^{-2} [WMO, 2008b]. Most of the SD data have been recorded with the Campbell-Stokes and Jordan sunshine recorders [Sanchez-Romero *et al.*, 2014] which consists of a spherical lens that focuses E onto a paper card, burning a trace if the irradiance exceeds the instrumental threshold [Stanhill, 2003; WMO, 2008b; Sanchez-Romero *et al.*, 2015]. The definition of a correct value for this threshold is not an easy issue: 120 W m^{-2} was proposed by WMO as resulting mean after some investigations performed at different stations, but it can vary between about 70 and 280 W m^{-2} depending on a number of factors such as the atmospheric turbidity and the moisture content of the paper card [WMO, 1969]. Some studies [Bider, 1958; Baumgartner, 1979] report that the burning threshold is on average higher in the early morning than in the late evening, because of dew or other water deposits on the glass sphere and on the paper card. This could produce notable losses in the daily SD values, especially in winter when temperatures are low and relative humidity is high [Painter, 1981].

The Campbell-Stokes SD measurements may be affected also by other problems [Brazdil *et al.*, 1994]. An example is a situation of very broken cloudiness. In this case, rapid bursts of high E , resulting in short periods during which $E_{g\downarrow}$ is reduced by clouds, may cause continuous traces [Painter, 1981; Kerr and Tabony, 2004]. In this way, an increase of TCC during the day may reduce $E_{g\downarrow}$ without affecting SD [Stanhill and Cohen, 2005]. A further limitation of SD measurements is that they are sensitive to atmospheric aerosols and water vapor [Oguz *et al.*, 2003; You *et al.*, 2010] only when E is close to the instrumental threshold, whereas $E_{g\downarrow}$ is sensitive to these variables especially when E is highest [Horseman *et al.*, 2008]. When E is close to the instrumental threshold, relative humidity can have an important influence on SD because it increases the size of particles via the aerosol hygroscopic effect and therefore changes their radiative properties [Tang, 1996; Baynard *et al.*, 2006; Qian *et al.*, 2007; Xia *et al.*, 2007]. In this case, E can fall under the instrumental threshold, and the paper card does not register any SD variation. It is however necessary to consider that SD and, especially, $E_{g\downarrow}$ measurements could also be affected by inhomogeneities, for example, due to instrument changes or recalibrations [Tang *et al.*, 2011; Wang *et al.*, 2012, 2015; Manara *et al.*, 2016a].

For all these reasons, it is not surprising that $E_{g\downarrow}$ and SD records do not always display consistent trends, as shown by studies which try to compare long-term trends of SD and $E_{g\downarrow}$ for different areas over the world (for a review, see Sanchez-Romero *et al.* [2014]). Thus, for example, Zhang *et al.* [2004] report a lower rate of decrease for SD than for $E_{g\downarrow}$ over the period 1961–2000 in Eastern China, while Liang and Xia [2005] and

Che et al. [2005], extending the study over the whole China for the same period, find a consistent spatial and temporal pattern for the two variables. *Stanhill and Kalma* [1995] also find a lower decrease for SD than for $E_{g\downarrow}$ in Hong Kong from 1958 to 1992, suggesting that long-term increase in aerosols induces a more significant reduction in $E_{g\downarrow}$ than in SD. However, more recent studies performed in China show that $E_{g\downarrow}$ trends may become weaker if quality-checked series are used [*Tang et al.*, 2010, 2011; *Wang et al.*, 2015]. Furthermore, stronger and more significant tendencies are reported for $E_{g\downarrow}$ than for SD in Germany. Specifically, *Liepert and Kukla* [1997] find a nonsignificant change in SD and a significant decrease of $E_{g\downarrow}$ between 1964 and 1990, while *Power* [2003] finds a nonsignificant trend in SD but an increase in $E_{g\downarrow}$ between the 1970s and the beginning of the 2000s. Similarly, *Stanhill and Cohen* [2005] in the United States and *Cutforth and Judiesch* [2007] in the Canadian Prairie find no long-term SD trend but a rather significant reduction of $E_{g\downarrow}$ during the last 50 years of the twentieth century. Moreover, *Soni et al.* [2012] find a significant and consistent decline for both variables during the 1971–2005 period in India. Overall, a large number of studies reported in the literature shows stronger tendencies for $E_{g\downarrow}$ than for SD even if every study presents regional peculiarities.

Recently, two homogenized data sets of SD [*Manara et al.*, 2015] and $E_{g\downarrow}$ [*Manara et al.*, 2016a] have been established for the first time for the Italian territory for the periods 1936–2013 and 1959–2013, respectively. Over the common period, both variables show a decreasing tendency until the mid-1980s and a subsequent increase until the end of the series. In Italy, as well as in the entire Mediterranean region, TCC shows higher values in the north than in the south and higher values in winter than in summer [*Enriquez-Alonso et al.*, 2016]. Owing to cloud-free conditions and high solar radiation intensity in summer, this region is particularly sensitive to air pollution showing one of the highest aerosol radiative forcing in the world [*Lelieveld et al.*, 2002].

In this context, this work aims to perform a detailed comparison of multidecadal SD and $E_{g\downarrow}$ variations in Italy [*Manara et al.*, 2015, 2016a] over the 1959–2013 period and to investigate the causes of their differences and the ability of SD to represent a good proxy variable to describe $E_{g\downarrow}$ multidecadal variations. The comparison is performed under all-sky (section 3) and clear-sky (section 4) conditions. Moreover, the agreement/disagreement in the obtained $E_{g\downarrow}$ and SD clear-sky records is discussed in relation to the variations estimated by means of a model based on Lambert-Beer's law and on a simple estimation of diffuse radiation (section 5). Finally, some conclusive remarks are given (section 6).

2. Data: Sunshine Duration and Global Radiation

The SD and $E_{g\downarrow}$ seasonal and annual all-sky records used in this paper are those presented by *Manara et al.* [2015] and *Manara et al.* [2016a]. They are northern and southern Italy average (relative) anomaly records obtained after projecting a large number of homogenized and gap-filled SD and $E_{g\downarrow}$ station anomaly records onto a 1° resolution grid (Figure 1).

The station records were obtained from different sources, mainly from the Council for Agricultural Research and Agricultural Economy Analysis (CREA—Consiglio per la ricerca in agricoltura e l'analisi dell'economia agraria) and the Italian Air Force (AM—Aeronautica Militare Italiana). Full details on data availability, on temporal homogeneity, gap-filling issues, and instruments are given in *Manara et al.* [2015, 2016a, 2016b, 2016c].

SD regional records cover a larger period than corresponding $E_{g\downarrow}$ records. However, here, we consider only the common period (1959–2013).

Beside all-sky records, we consider corresponding clear-sky $E_{g\downarrow}$ and SD records. Specifically, clear-sky days were selected starting from an updated version of the TCC database presented by *Maugeri et al.* [2001] and considering only the days with a daily TCC mean lower than or equal to 1 okta. The advantage of 1 okta as the threshold instead of 0 okta (real clear-sky days) is a higher number of days and more robust clear-sky records even if the selected days are not completely clear. Nevertheless, this choice does not introduce significant differences in the regional records of Italy [*Manara et al.*, 2016a].

As clear-sky records may contain only a small number of days, monthly averages may be influenced by the dates in which these days fall, especially in spring and autumn. Thus, we transformed the daily $E_{g\downarrow}$ data into clearness index data and the daily SD data into relative SD data. This step allows removing the influence of the solar zenith angle and making the corresponding monthly mean not influenced by the dates in which the values fall. The monthly records were then gap-filled and retransformed into absolute records using

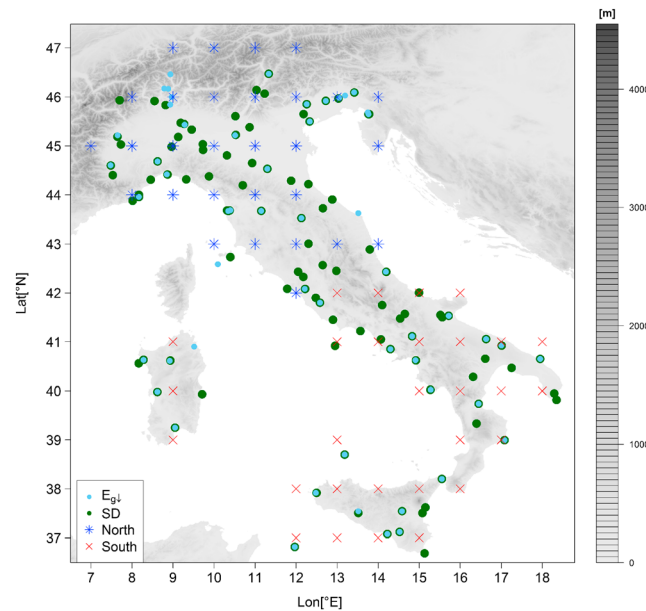


Figure 1. Spatial distribution of SD (green points) and $E_{g\downarrow}$ (light blue points) station records and of the grid-mode version of the data set. Blue stars and red crosses represent, respectively, northern and southern Italy grid points. The figure also shows the orography of the region.

the exo-atmospheric value relative to the central day of the corresponding month. Then, seasonal and annual anomaly series were projected onto the same grid considered for the all-sky records (Figure 1) and averaged in order to obtain northern and southern Italy SD and $E_{g\downarrow}$ seasonal and annual clear-sky anomaly records.

3. Comparison Between Sunshine Duration and Global Radiation Records Under All-Sky Conditions

The northern and southern Italy annual and seasonal SD and $E_{g\downarrow}$ records obtained under all-sky conditions are shown in Figure 2, together with corresponding Gaussian low-pass filters.

In order to better compare SD and $E_{g\downarrow}$ records, we also show the $E_{g\downarrow}/SD$

ratio records (Figure 3—black line) and the corresponding running trend analysis (Figure 4) [Brunetti *et al.*, 2006]. The latter allows estimating the significance and the slope of the trend of these records for each subinterval of at least 21 years, with significance estimated by means of the Mann-Kendall nonparametric test and slope computed using the Theil-Sen method [Theil, 1950; Sen, 1968]. The idea of investigating the $E_{g\downarrow}/SD$ ratios is that any trend in these records reflects the differences in the trends of SD and $E_{g\downarrow}$. Figures 2 and 3 highlight relevant differences between the SD and $E_{g\downarrow}$ records (see Manara *et al.* [2015, 2016a] for a detailed discussion of trends). Overall, SD records show a higher interannual variability than $E_{g\downarrow}$ ones (Figure 2), which is probably a consequence of the higher influence of cloudiness on SD day-to-day variability. Specifically, changes in cloud amount directly diminish or enhance SD, whereas for $E_{g\downarrow}$ a decrease of the direct fraction is partially compensated by an increase of the diffuse fraction and vice versa [Lohmann *et al.*, 2006]. In fact, the discrepancy is maximum in winter (the standard deviation of the residuals from the low-pass filter being 0.07 for $E_{g\downarrow}$ and 0.14 for SD in the northern region and 0.06 for $E_{g\downarrow}$ and 0.10 for SD in the southern region) and minimum in summer (0.02 for $E_{g\downarrow}$ and 0.04 for SD in the northern region and 0.03 for both variables in the southern region) when cloudiness is minimum and frequency of clear-sky days is maximum.

The agreement between SD and $E_{g\downarrow}$ decadal variability and long-term trends depends on the considered region, season, and period. Specifically, annual SD series present a similar decadal variability to $E_{g\downarrow}$ series (Figure 2) showing a dimming/brightening sequence. However, the dimming period for SD is shorter and less intense with respect to $E_{g\downarrow}$. This is highlighted also by the decrease (stronger in the north than in the south) observed in the ratio records until the end of the 1980s (Figure 3). Therefore, the ratio records for the longest subperiods (Figure 4) have significant negative trend (about $-1.5\% \text{decade}^{-1}$). Moreover, the SD series show a trend inversion from dimming to brightening at the end of the 1970s/beginning of the 1980s while the $E_{g\downarrow}$ series show it around the mid-1980s (Figure 2).

During winter the two variables show strong differences until the mid-1980s (Figure 2), especially in the north, where SD does not show a decreasing tendency in the dimming period whereas $E_{g\downarrow}$ does. This is also highlighted by the decrease in the ratio records (Figure 3) and by the correlation coefficients (Table 1) between the low-pass filters of the two variables that are negative in the north (-0.22) and positive, but rather low, in the south (0.60). Nevertheless, the correlation coefficients of the residuals from the low-pass filters are very high and significant in both regions (0.96 for the north and 0.83 for the south) underlining a

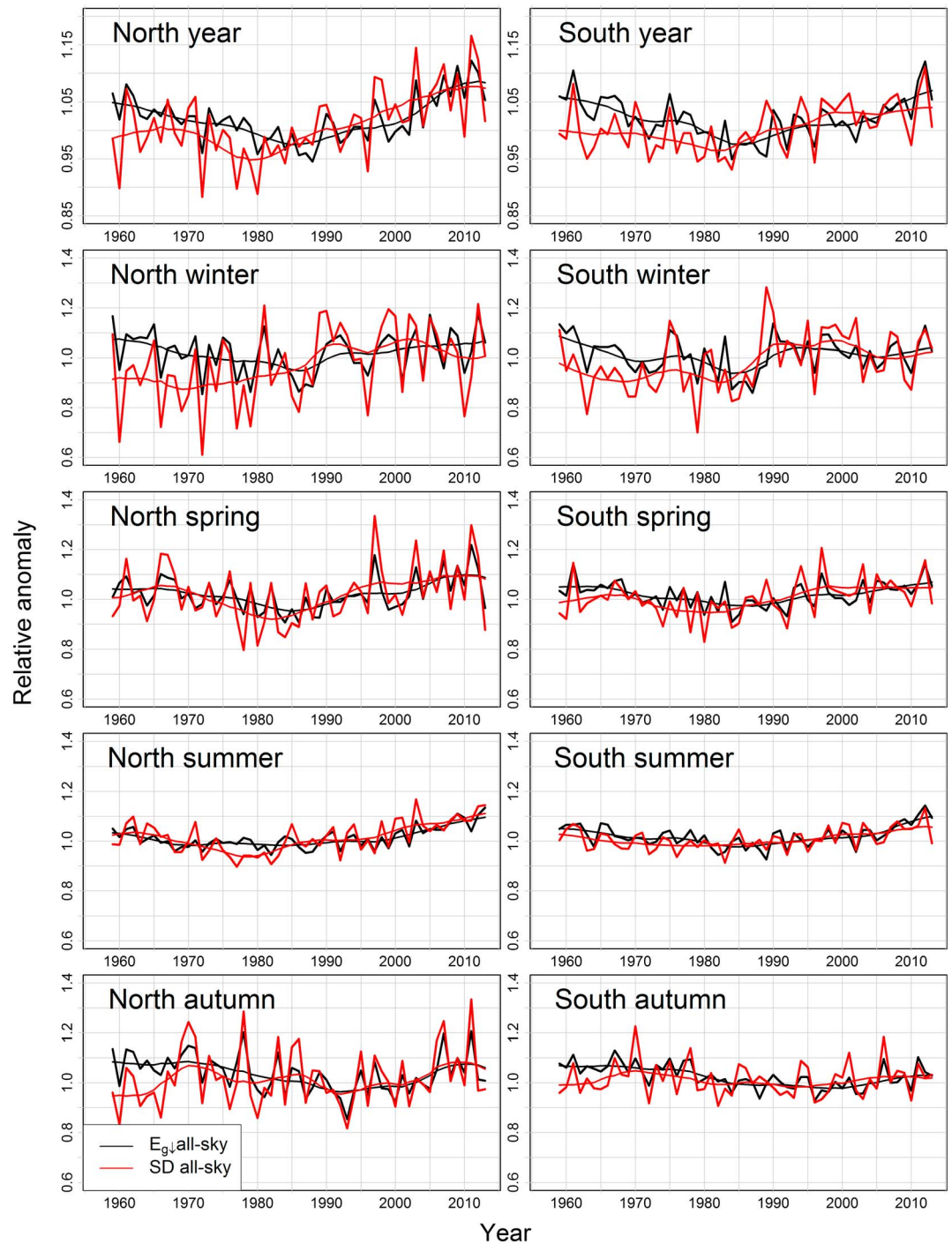


Figure 2. (left) Northern and (right) southern Italy annual and seasonal SD (red line) and $E_{g\downarrow}$ (black line) records obtained under all-sky conditions, plotted together with 11 year window, 3 year standard deviation Gaussian low-pass filters. The series are expressed as relative deviations from the 1976 to 2005 averages. Annual graphs are shown with an expanded scale with respect to seasonal ones.

good agreement in terms of year-to-year variability. The agreement of low-pass filters is better during the brightening period, where both variables increase (Figure 4). During spring and summer both variables show a decadal variability similar to the annual mean (Figure 2), and the ratio records show that the discrepancies between SD and $E_{g\downarrow}$ records are less evident compared to the winter ones (Figures 3 and 4). However, SD shows a trend inversion at the beginning of the 1980s while $E_{g\downarrow}$ shows it around the mid-1980s

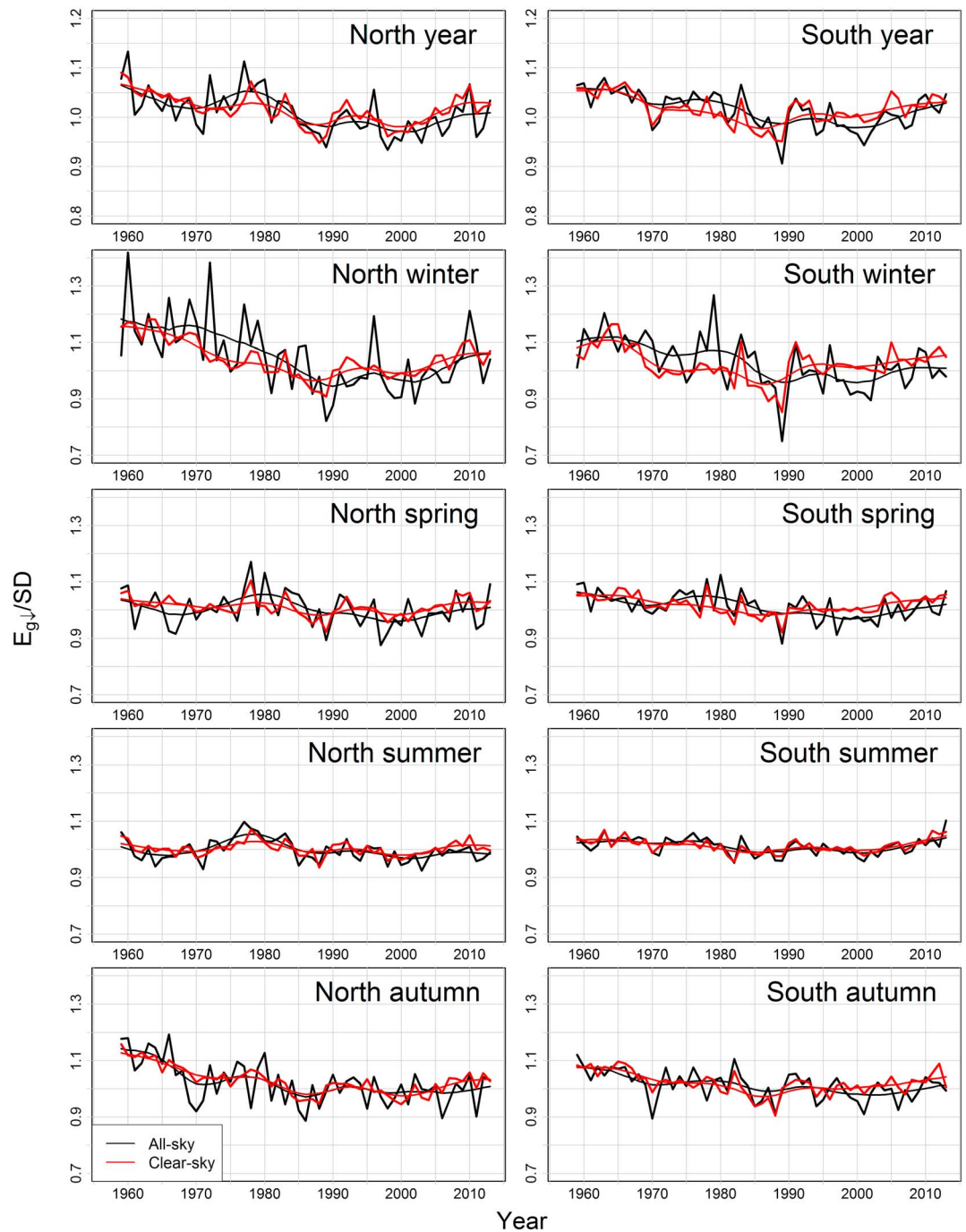


Figure 3. Annual and seasonal $E_{g\downarrow}/SD$ records for (left) northern and (right) southern Italy under all-sky (black line) and clear-sky (red line—see section 4) conditions. The series are plotted together with an 11 year window, 3 year standard deviation Gaussian low-pass filter. Annual graphs are shown with an expanded scale with respect to seasonal ones.

(Figure 2). Moreover, in the northern region, SD has a stronger decrease than $E_{g\downarrow}$ in the 1970s and a stronger increase in the 1980s and 1990s, which causes the corresponding increase/decrease in the ratio records. However, the increase in the ratio record is very short and has a significant trend only for few subperiods (Figure 4). In the southern region, in the dimming period both in spring and summer, SD has a lower decrease than $E_{g\downarrow}$, which causes a decrease (stronger in spring) of the ratio records (Figures 3 and 4). Interestingly, the best agreement between the two variables in terms of variability at decadal timescale concerns summer that is the season in which the correlation coefficients between SD and $E_{g\downarrow}$ residuals are

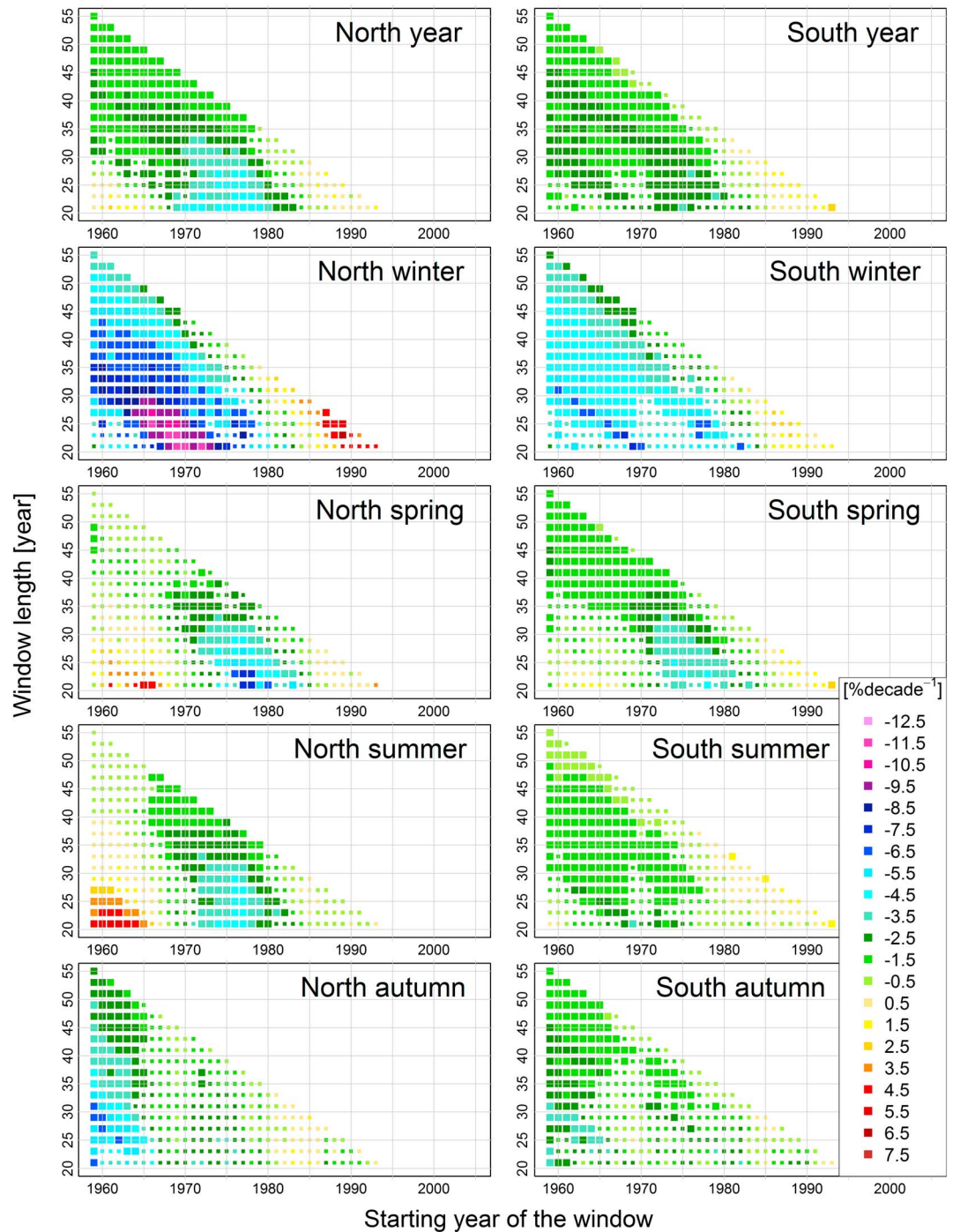


Figure 4. Trend of the all-sky $E_{g\downarrow}/SD$ records for each subinterval of at least 21 years. The results are reported both in terms of slopes ($\% \text{ decade}^{-1}$ —pixel color) and significance levels (large pixels: $p \leq 0.05$; small pixels: $p > 0.05$). The y axis represents the window width, and the x axis represents the starting year of the window used for the computation of the trend.

lowest (Table 1). On the contrary, the lowest agreement between the low-pass filter records (winter in northern Italy over the 1959–2013 period) corresponds to a very high correlation coefficient (0.92) of the residuals, giving evidence that the processes causing the agreement/disagreement of SD and $E_{g\downarrow}$ may be different at yearly and decadal timescales.

During autumn, the two variables show a good agreement even if there are strong differences (more pronounced in the north) in the first decade where SD records increase while $E_{g\downarrow}$ ones decrease (Figure 2).

Table 1. Correlation Coefficients Between SD and $E_{g\downarrow}$ Records (Anomalies, Low Pass Filters, and Residuals From the Filters) for Northern and Southern Italy Under All-Sky and Clear-Sky (See Section 4) Conditions^a

| | Year | Year | | | Winter | | | Spring | | | Summer | | | Autumn | | |
|-----------|-------|-----------|--------|----------|-------------|--------|----------|-------------|--------|----------|-------------|--------|----------|-------------|--------|-------------|
| | | Anomaly | Filter | Residual | Anomaly | Filter | Residual | Anomaly | Filter | Residual | Anomaly | Filter | Residual | Anomaly | Filter | Residual |
| All-sky | North | 1959–2013 | 0.73 | 0.73 | 0.83 | 0.77 | 0.18 | 0.92 | 0.90 | 0.89 | 0.93 | 0.81 | 0.89 | 0.77 | 0.39 | 0.92 |
| | | 1959–1985 | 0.72 | 0.73 | 0.85 | 0.85 | -0.22 | 0.96 | 0.93 | 0.93 | 0.94 | 0.65 | 0.72 | 0.71 | -0.10 | 0.92 |
| | | 1986–2013 | 0.82 | 0.96 | 0.83 | 0.80 | 0.32 | 0.87 | 0.89 | 0.93 | 0.93 | 0.89 | 0.97 | 0.84 | 0.91 | 0.91 |
| Clear-sky | South | 1959–2013 | 0.56 | 0.48 | 0.66 | 0.67 | 0.41 | 0.76 | 0.77 | 0.65 | 0.85 | 0.75 | 0.84 | 0.76 | 0.54 | 0.79 |
| | | 1959–1985 | 0.72 | 0.89 | 0.75 | 0.80 | 0.60 | 0.83 | 0.84 | 0.86 | 0.85 | 0.71 | 0.86 | 0.72 | 0.40 | 0.82 |
| | | 1986–2013 | 0.61 | 0.85 | 0.59 | 0.67 | 0.70 | 0.68 | 0.78 | 0.84 | 0.84 | 0.80 | 0.95 | 0.79 | 0.74 | 0.78 |
| Clear-sky | North | 1959–2013 | 0.50 | 0.65 | 0.10 | 0.08 | 0.01 | 0.26 | 0.58 | 0.84 | 0.31 | 0.64 | 0.86 | 0.06 | 0.28 | 0.42 |
| | | 1959–1985 | 0.55 | 0.78 | -0.04 | -0.08 | -0.62 | 0.25 | 0.60 | 0.91 | 0.17 | 0.47 | 0.80 | 0.13 | 0.37 | 0.20 |
| | | 1986–2013 | 0.73 | 0.91 | 0.20 | 0.52 | 0.84 | 0.28 | 0.67 | 0.95 | 0.43 | 0.75 | 0.94 | 0.00 | 0.71 | 0.52 |
| Clear-sky | South | 1959–2013 | 0.63 | 0.88 | 0.33 | 0.16 | 0.31 | 0.12 | 0.61 | 0.89 | 0.39 | 0.79 | 0.93 | 0.51 | 0.44 | 0.08 |
| | | 1959–1985 | 0.72 | 0.94 | 0.39 | 0.04 | -0.13 | 0.02 | 0.63 | 0.98 | 0.34 | 0.80 | 0.99 | 0.46 | 0.49 | 0.01 |
| | | 1986–2013 | 0.61 | 0.96 | 0.26 | 0.30 | 0.85 | 0.19 | 0.64 | 0.97 | 0.46 | 0.80 | 0.92 | 0.56 | 0.37 | 0.12 |

^aSignificance level is given only for the correlation between the residual series: Bold $p \leq 0.05$, italic $0.05 < p \leq 0.1$, and roman $p > 0.1$. Periods were selected in according to the dimming and brightening periods illustrated by Manara et al. [2016a].

Table 2. SD and $E_{g\downarrow}$ Trends in Northern and Southern Italy Under All-Sky and Clear-Sky (See Section 4) Conditions^a

| | | | Year | Winter | Spring | Summer | Autumn |
|-----------------|-----------|-------------------|-------------|-------------|-------------|-------------|-------------|
| North all-sky | 1959–2013 | $E_{g\downarrow}$ | + | + | + | 1.2 | −1.6 |
| | | SD | 1.7 | 3.5 | + | 2.0 | + |
| | 1959–1980 | $E_{g\downarrow}$ | −2.4 | −6.5 | −2.9 | −2.0 | − |
| | | SD | − | − | − | −5.9 | + |
| | 1985–2013 | $E_{g\downarrow}$ | 4.4 | 5.1 | 5.8 | 4.7 | + |
| | | SD | 3.6 | + | 5.5 | 4.2 | + |
| South all-sky | 1959–2013 | $E_{g\downarrow}$ | − | − | + | + | −1.7 |
| | | SD | 1.1 | 2.4 | 1.4 | 0.9 | − |
| | 1959–1980 | $E_{g\downarrow}$ | −2.9 | −5.6 | −3.5 | −2.2 | − |
| | | SD | − | − | − | − | + |
| | 1985–2013 | $E_{g\downarrow}$ | 3.0 | + | 3.5 | 4.3 | + |
| | | SD | 1.9 | + | 2.5 | 2.3 | + |
| North clear-sky | 1959–2013 | $E_{g\downarrow}$ | − | − | − | + | −1.1 |
| | | SD | 0.9 | 1.6 | 0.6 | 0.8 | 1.1 |
| | 1959–1980 | $E_{g\downarrow}$ | −3.2 | −5.2 | −2.5 | −1.4 | −5.6 |
| | | SD | − | 2.2 | −2.1 | −2.0 | − |
| | 1985–2013 | $E_{g\downarrow}$ | 4.3 | 5.7 | 3.8 | 3.7 | 4.4 |
| | | SD | 2.2 | 1.7 | 1.8 | 3.0 | 2.7 |
| South clear-sky | 1959–2013 | $E_{g\downarrow}$ | − | − | − | − | −1.2 |
| | | SD | + | 0.6 | + | + | − |
| | 1959–1980 | $E_{g\downarrow}$ | −3.6 | −4.5 | −4.0 | −2.9 | −4.0 |
| | | SD | −0.9 | + | −1.6 | −1.8 | − |
| | 1985–2013 | $E_{g\downarrow}$ | 3.5 | 4.6 | 3.8 | 3.6 | 3.2 |
| | | SD | 1.2 | 1.0 | 1.2 | 1.9 | 0.9 |

^aValues are expressed in %decade^{−1}. Values are shown in roman for significance level of 0.05 < p ≤ 0.1 and in bold for a significance level of p ≤ 0.05. For nonsignificant trends, only the sign of the slope is given. The significance of the trends is evaluated with the Mann-Kendall nonparametric test while the trends are estimated by the Theil-Sen method. Periods were selected according to the dimming and brightening obtained for both variables.

This is reflected by a clear decrease in the ratio records (Figure 3) that continues until the mid-1980s (even if the slope is weaker) due to a stronger dimming in the $E_{g\downarrow}$ records than in the SD ones. The agreement is higher if the subsequent part of the series is considered (Table 1 and Figure 2).

The Theil-Sen method trends, estimated for some relevant periods, confirm what has already been discussed above (Table 2) showing stronger (or comparable) and more significant trends for $E_{g\downarrow}$ than SD. The only exceptions are autumn (nonsignificant trend) for both regions, summer in the north (stronger SD trend than $E_{g\downarrow}$) during the dimming period, and winter in the south (nonsignificant trend) for the brightening period.

4. Comparison Between Sunshine Duration and Global Radiation Records Under Clear-Sky Conditions

Analyzing factors causing different decadal variability and long-term trends in SD and $E_{g\downarrow}$ records is a challenge, as in addition to instrumental issues, a number of environmental variables should be considered including cloudiness, atmospheric aerosols, and relative humidity. One approach to reduce the complexity of the problem is to remove cloudiness effect selecting only clear-sky days.

The $E_{g\downarrow}$ clear-sky records (Figure 5) indicate a well-defined dimming/brightening sequence with a rather coherent decadal variability and a transition from dimming to brightening around the mid-1980s [Manara et al., 2016a]. The removal of cloud contribution produces on SD records (Figure 5) an effect already observed in the $E_{g\downarrow}$ case [Manara et al., 2016a]: the dimming period becomes longer and the corresponding trends more significant with the only exception of winter. Moreover, the increase during the brightening period (spring and summer) becomes weaker. The most relevant changes are observed in autumn when under all-sky conditions the SD curves do not show any signal, while under clear-sky conditions dimming and brightening periods become significant. The trend is more pronounced during the dimming period in the

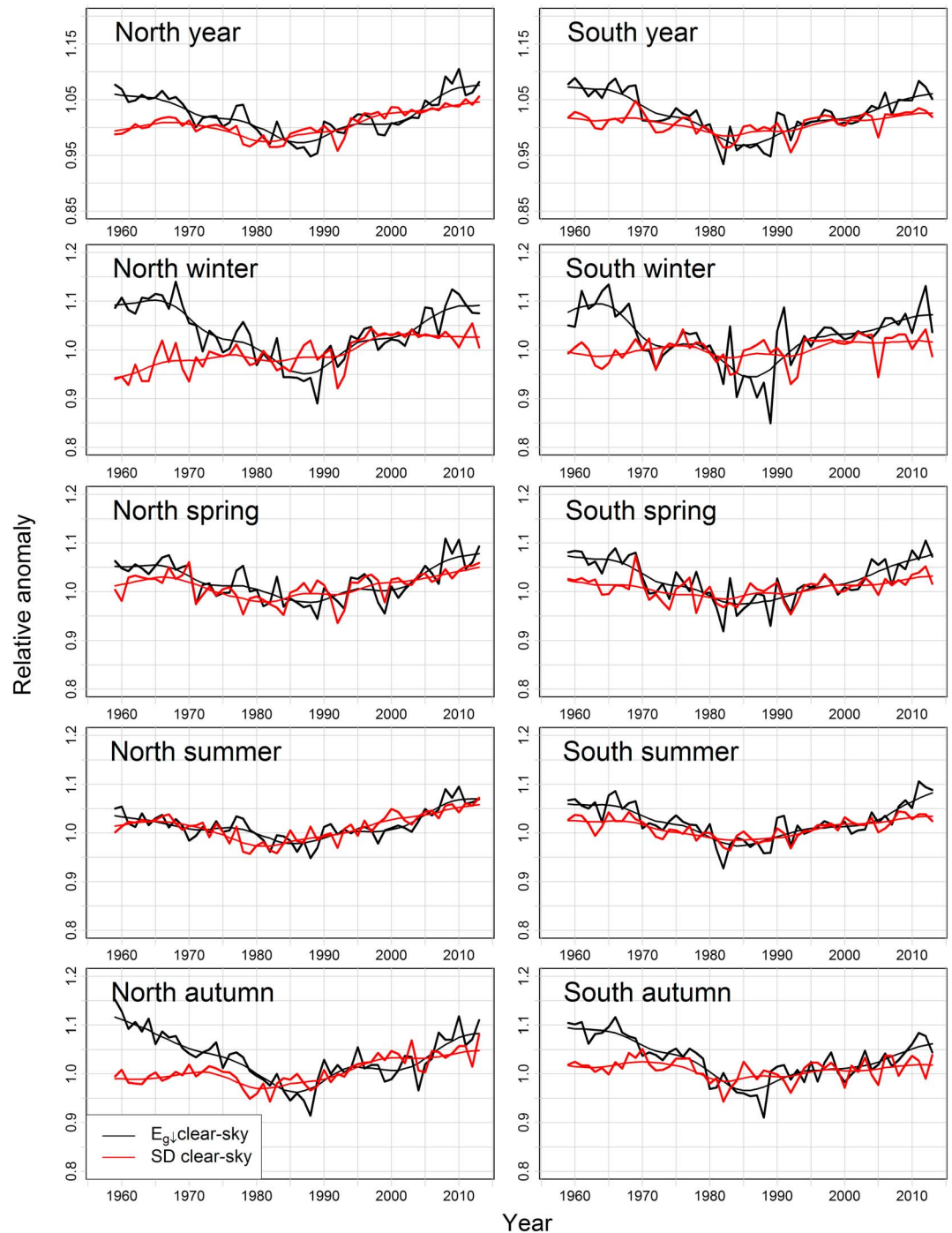


Figure 5. (left) Northern and (right) southern Italy annual and seasonal SD (red line) and $E_{g\downarrow}$ (black line) records obtained under clear-sky conditions, plotted together with 11 year window, 3 year standard deviation Gaussian low-pass filters. The series are expressed as relative deviations from the 1976 to 2005 averages. Annual graphs are shown with an expanded scale with respect to seasonal ones.

south (e.g., $-1.1\% \text{decade}^{-1}$, p value ≤ 0.05 over the period 1959–1985) and during the brightening period in the north (Table 2).

Differently from the all-sky records, the clear-sky $E_{g\downarrow}$ records show a comparable (in the north) or slightly higher (in the south) interannual variability than the SD ones over the period 1959–2013. The standard deviations of the residuals from the low-pass filters range from 0.014 (summer in the north) to 0.034 (winter in the

south) for $E_{g\downarrow}$ and from 0.010 (annual mean in the north) to 0.022 (winter in the south) for SD. Moreover, the interannual variability is lower for the clear-sky than for the all-sky records, which is an obvious consequence of the relevant role of cloudiness in the year-to-year variability of these variables. It is interesting to highlight that the SD and $E_{g\downarrow}$ residuals from the filters have rather low correlations in clear-sky compared to the all-sky conditions. The highest correlation coefficients for the residuals are observed in spring for both regions, autumn in the north, and summer in the south (Table 1). However, the common variance between the SD and $E_{g\downarrow}$ residuals is rather low, and only few correlation coefficients are significant. Moreover, in most seasons and periods under clear-sky conditions, correlation between filters is comparable or increases with respect to all-sky conditions (Table 1). This underlines that under clear-sky conditions SD and $E_{g\downarrow}$ are affected by the same factors at decadal timescale, even though their agreement in terms of year-to-year variability is rather low.

As already observed for all-sky conditions, the agreement between clear-sky SD and $E_{g\downarrow}$ decadal variability and long-term trends depends on the considered region, season, and period (Figure 5). The ratio records show, as already discussed for the all-sky series, a decreasing tendency until the mid-1980s (more pronounced in winter and autumn) resulting from a stronger dimming of $E_{g\downarrow}$ than of SD (Table 2). The corresponding running trend analysis (Figure 6) shows significant trends for almost all subperiods starting in the first decade, which was not the case in the all-sky conditions (Figure 4) where the decrease was significant only when longer periods were considered. The agreement between the two variables is higher in the brightening period as both variables increase, even if the $E_{g\downarrow}$ trends present higher values (Table 2). This is reflected in some positive subperiods in the last part of the ratio records (Figure 6) differently from the all-sky conditions (Figure 4) when very few subperiods showed a significant trend.

It is interesting to underline that in northern Italy, during summer, the decrease of the first period in the ratio record is not present and only few subperiods have a significant trend, implying a good agreement between SD and $E_{g\downarrow}$. Here the few subperiods with a significant negative trend are due to different reversal years from dimming to brightening for SD (beginning of 1980s) and $E_{g\downarrow}$ (mid-1980s). It is worth noting that this is the only case (as already observed under all-sky conditions) in which SD shows a stronger dimming than $E_{g\downarrow}$ (Table 2) as highlighted by the only case in which the running trend analysis shows subperiods with positive trend during the 1960s (Figure 6).

5. Sunshine Duration and Global Radiation Sensitivity to Variations in Atmospheric Turbidity

The main result highlighted by the comparison between the SD and $E_{g\downarrow}$ clear-sky records is that the latter shows generally stronger signals than the former, with a stronger decrease in the dimming period and a slightly stronger increase in the brightening period (the only exception is summer in northern Italy).

In order to investigate whether such behavior can be explained by a different sensitivity of SD and $E_{g\downarrow}$ to atmospheric turbidity variations, we applied a model based both on Lambert-Beer's law and on a simple estimation of diffuse radiation.

The model we applied is based on *Rigollier et al.* [2000]. It estimates the atmospheric attenuation of $E_{g\downarrow}$ (calculating separately the direct (E) and the diffuse ($E_{d\downarrow}$) components) under clear-sky conditions, in terms of the atmospheric turbidity. Indeed, the larger the atmospheric turbidity, the larger the attenuation of the direct radiation (less E) and the larger the portion of scattered radiation (more $E_{d\downarrow}$) by the atmosphere.

In this model, E is calculated with the following equation [*Rigollier et al.*, 2000]:

$$E(\phi, k) = I_0 \cdot E_0(k) \cdot \int_{\omega_{SR}(\phi, k)}^{\omega_{SS}(\phi, k)} \cos(\theta_{INC}(\phi, k, \omega)) \cdot e^{-0.8662 \cdot T_L \cdot m_A(\phi, k, \omega) \cdot \delta_R(\phi, k, \omega)} d\omega \quad (1)$$

Specifically, ϕ is the latitude of the considered point; k ($k = 1, \dots, 12$) is the considered month; I_0 is the solar constant ($I_0 = 1361 \text{ W m}^{-2}$ [*Kopp and Lean*, 2011]); $E_0(k)$ is the eccentricity factor [*Iqbal*, 1983]; $\theta_{INC}(\phi, k, \omega)$ is the solar angle of incidence for a flat surface [*Iqbal*, 1983]; T_L is the turbidity Linke factor, i.e., the number of clean dry atmospheres that would be necessary to pile up in order to obtain the same attenuation of the extraterrestrial radiation as that produced by the actual atmosphere, is related to the total turbidity (aerosol and water vapor) [*Jacovides*, 1997], and is considered standardized (by means of the 0.8662 factor) for an air mass equal to 2 [*Grenier et al.*, 1995]; $m_A(\phi, k, \omega)$ is the optical air mass [*Jacovides*, 1997; *Rigollier et al.*, 2000]; and $\delta_R(\phi, k, \omega)$ is the Rayleigh optical depth [*Rigollier et al.*, 2000].

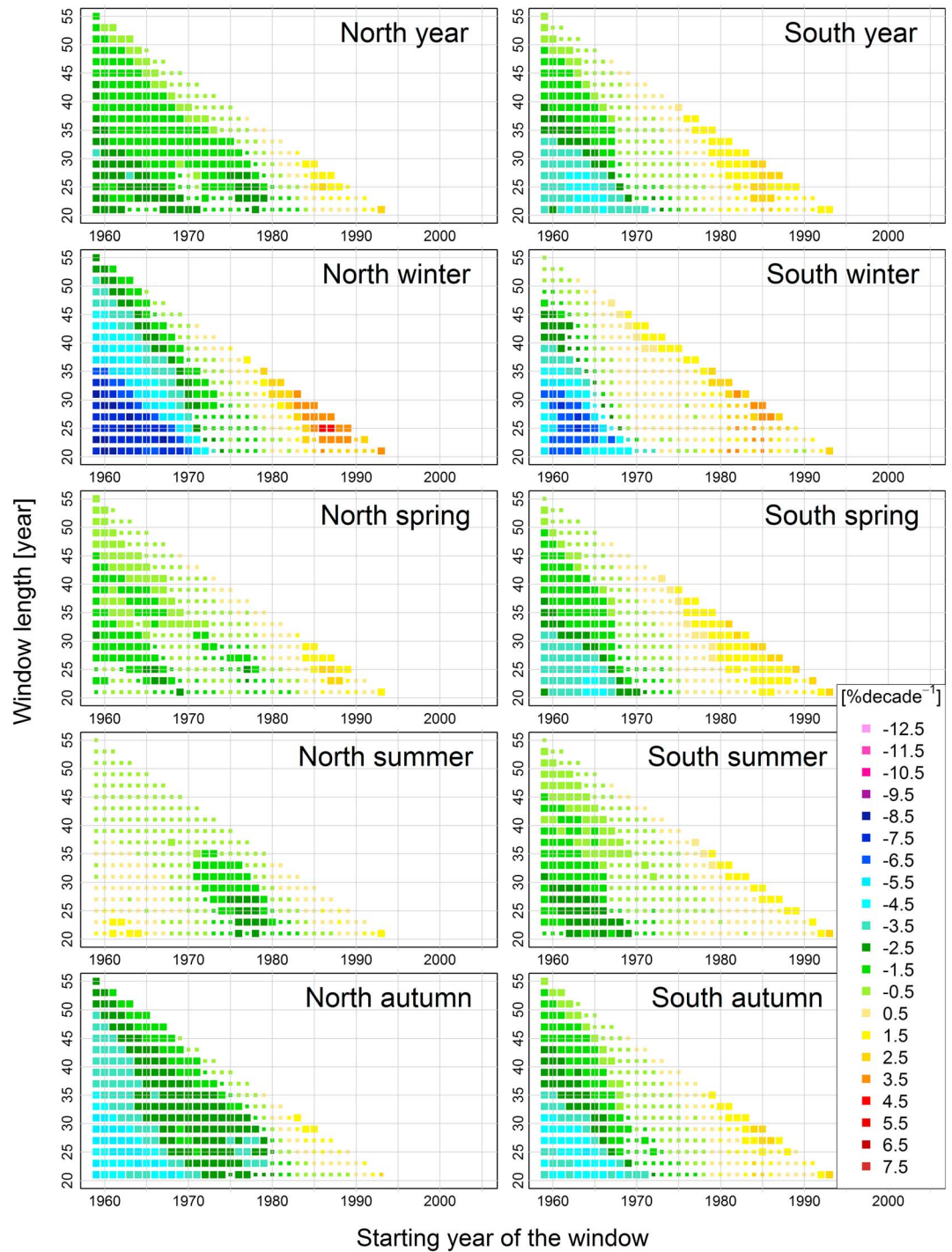


Figure 6. Trend of the clear-sky E_{GI}/SD records for each subinterval of at least 21 years. The results are reported both in terms of slopes ($\% \text{ decade}^{-1}$ —pixel color) and significance levels (large pixels: $p \leq 0.05$; small pixels: $p > 0.05$). The y axis represents the window width, and the x axis represents the starting year of the window used for the computation of the trend.

The equation is considered for the central day of each month, and the integration is performed dividing the length of the day (from sunrise ($\omega_{SR}(\phi, k)$) to sunset ($\omega_{SS}(\phi, k)$)) in N intervals (expressed in hour angle— ω). In order to avoid rounding errors, we used a very short time step ($N = 100,000$).

In the Campbell-Stokes SD recorder, the paper card is always normal to the direct radiation, and therefore, the term $\cos(\theta_{INC}(\phi, k, \omega))$ in equation (1) is equal to 1. Specifically, all time steps for which the direct radiation is

higher than 120 W m^{-2} are selected, and the difference between the hour angles corresponding to the maximum and the minimum steps are transformed in hours.

Differently, to calculate E , the term $\cos(\theta_{\text{INC}}(\phi, k, \omega))$ is different for each time step, and so the daily value is calculated integrating equation (1) from sunrise to sunset. $E_{\text{d}\downarrow}$ is obtained integrating the following equation from sunrise to sunset [Rigollier et al., 2000]:

$$E_{\text{d}\downarrow}(T_L, \phi, k, \omega) = I_0 \cdot E_0(k) \cdot T_{\text{rd}}(T_L) \cdot F_{\text{d}}(T_L, \phi, k, \omega) \quad (2)$$

where $T_{\text{rd}}(T_L)$ is the diffuse transmission function at zenith and $F_{\text{d}}(T_L, \phi, k, \omega)$ is the diffuse angular function as given in the following equations:

$$T_{\text{rd}}(T_L) = -1.5843 \cdot 10^{-2} + 3.0543 \cdot 10^{-2} \times T_L + 3.797 \cdot 10^{-4} \cdot T_L^2 \quad (3)$$

$$F_{\text{d}}(T_L, \phi, k, \omega) = A_0(T_L) + A_1(T_L) \cdot \sin(h(\phi, k, \omega)) + A_2(T_L) \cdot (\sin(h(\phi, k, \omega)))^2 \quad (4)$$

where $h(\phi, k, \omega)$ is the solar altitude angle and the coefficients are set as follows:

$$\begin{cases} A_0(T_L) = 2.6463 \cdot 10^{-1} - 6.1581 \cdot 10^{-2} \cdot T_L + 3.1408 \cdot 10^{-3} \cdot T_L^2 \\ A_1(T_L) = 2.0402 + 1.8945 \cdot 10^{-2} \cdot T_L - 1.1161 \cdot 10^{-2} \cdot T_L^2 \\ A_2(T_L) = -1.3025 + 3.9231 \cdot 10^{-2} \cdot T_L + 8.5079 \cdot 10^{-3} \cdot T_L^2 \end{cases} \quad (5)$$

$A_0(T_L)$ is subjected to the following condition:

$$\text{if } (A_0(T_L) \cdot T_{\text{dr}}(T_L)) < 2 \cdot 10^{-3}, A_0(T_L) = \frac{2 \cdot 10^{-3}}{T_{\text{dr}}(T_L)} \quad (6)$$

This additional condition is necessary because $A_0(T_L)$ becomes negative for $T_L > 6$.

At first, we applied equations (1) and (2) to estimate the T_L monthly values at each site. Specifically, we searched for the T_L values which give the observed clear-sky $E_{\text{g}\downarrow}$ monthly means over the period 1959–2013. However, such estimation may have some problems as all the data preprocessing has been performed to ensure the accuracy and temporal homogeneity of anomaly records, whereas possible problems of the absolute records have not been considered. We can therefore not exclude the presence of small biases, e.g., due to the fact that the sky-view factor can be partially reduced during the sunrise/sunset in some stations. This could be true for the stations surrounded by hills and mountains or located in urban areas (e.g., records that are collected at urban observatories). Moreover, it should be considered that the T_L values are calculated comparing the simulated $E_{\text{g}\downarrow}$ values with the observed clear-sky $E_{\text{g}\downarrow}$ means obtained using 1 okta as threshold. The monthly T_L values we get with this estimation have therefore to be considered only as indicative. The obtained values for southern Italy are about 15–20% lower than the northern Italy ones. The means over all Italian stations range from 3.4 (January) to 5.5 (July). Considering that the observed clear-sky $E_{\text{g}\downarrow}$ means could be slightly underestimated, it is reasonable to consider for Italy the following T_L values: about 3 in winter, 5 in summer and 4 in spring and autumn. This small correction corresponds to the assumption that the actual $E_{\text{g}\downarrow}$ means are 2–3% higher than those we get from our clear-sky records.

These T_L values correspond however to $E_{\text{g}\downarrow}$ means over the entire 1959–2013 period. In order to estimate realistic T_L values for shorter intervals as well, we have to consider that during the dimming period, T_L values increased until they reached their maximum values and then they decreased during the brightening period down to their final values. We considered therefore as predimming T_L values those that justify the $E_{\text{g}\downarrow}$ means in the first years (obtained starting from the $E_{\text{g}\downarrow}$ 1959–2013 means and the relative anomalies—with respect to the 1959–2013 period—of the first years). Then, we used the same approach to identify the most realistic prebrightening T_L values and the values of the last years.

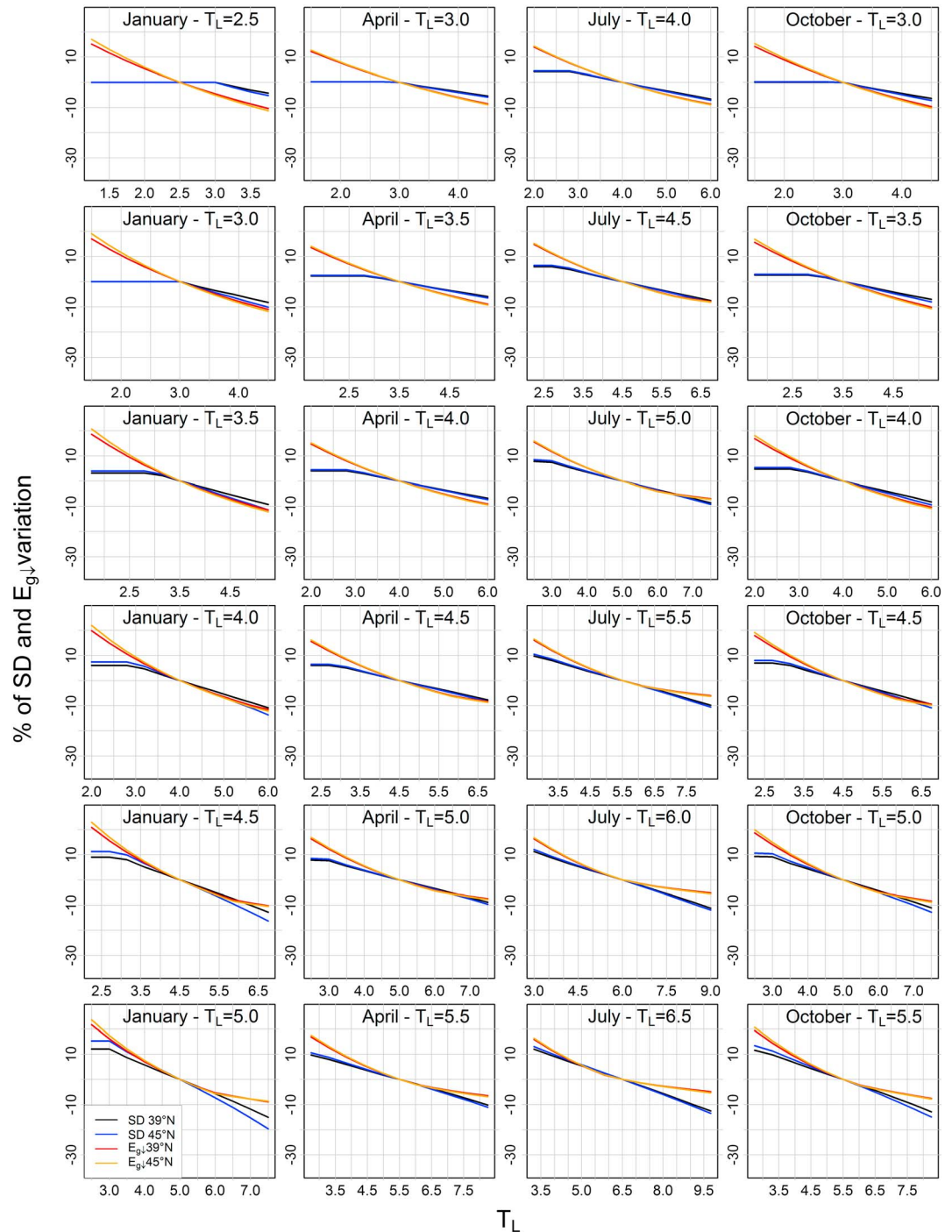


Figure 7. Variation (expressed in percentage) of modeled SD ($E_{g\downarrow}$) for a T_L increase/decrease in relation to the starting value indicated in each plot. The black (blue) line represents SD variations while the red (orange) line represents $E_{g\downarrow}$ variations for a point located at a latitude of 39°N (45°N). Results refer to the central month of each season.

Then, we analyzed SD and $E_{g\downarrow}$ sensitivity to T_L variations by means of equations (1) and (2). Specifically, we considered two points located at sea level and representative of northern and southern latitudes (45°N and 39°N respectively), and we calculated variations of SD and $E_{g\downarrow}$ for a T_L increase/decrease with respect to each integer and half of integer comprised in a wide interval of values. We report the results in Figure 7 for the central month of each season (January, April, July, and October) and for T_L starting values ranging from the predimming to the prebrightening values, estimated above.

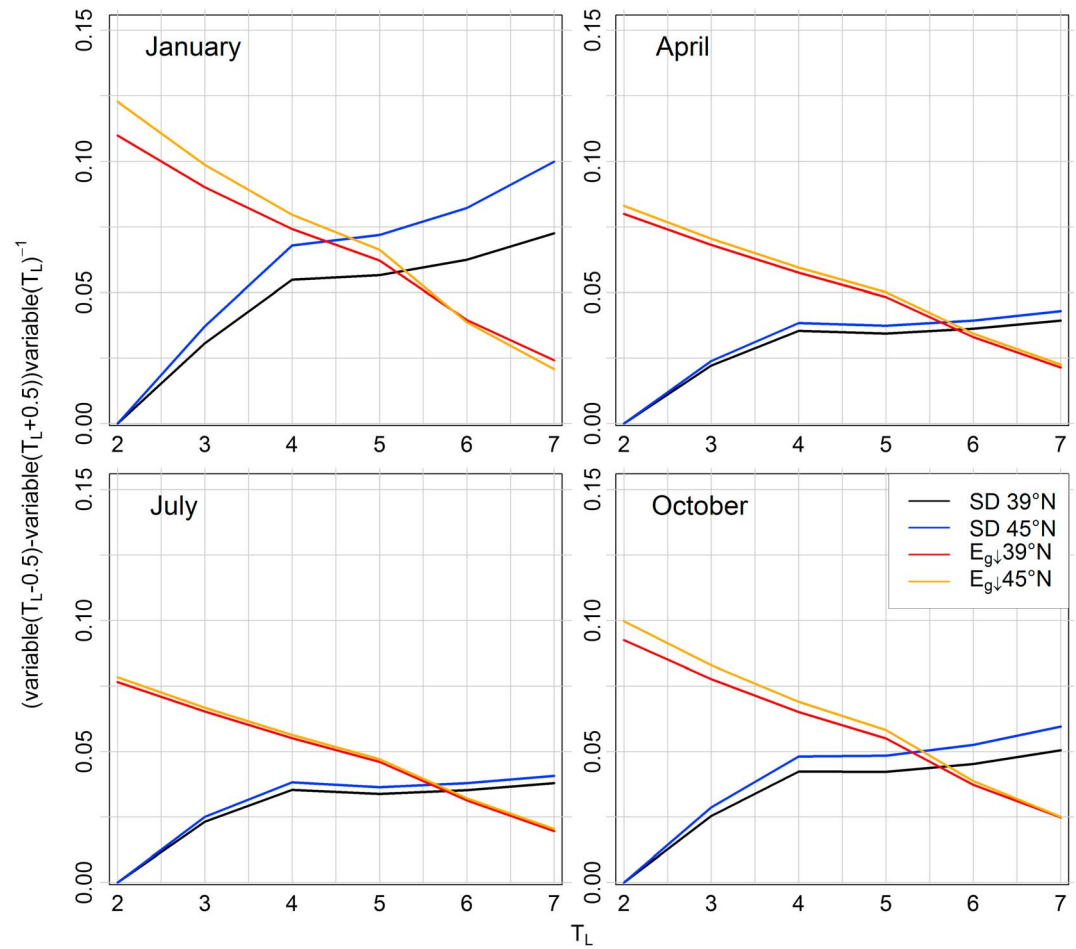


Figure 8. Relative decrease of modeled SD ($E_{g\downarrow}$) for each integer T_L in the range 2–7 for T_L increasing from $T_L - 0.5$ to $T_L + 0.5$. The black (blue) line represents SD variations while the red (orange) line represents $E_{g\downarrow}$ variations for a point located at a latitude of 39°N (45°N). Results refer to the central month of each season.

The curves show a latitudinal effect almost only for SD in winter and autumn for T_L starting values higher than 4 with stronger variations for the point located at a higher latitude. We discuss therefore the figure without differentiating the lines concerning the two latitudes.

In spring (April), considering a predimming T_L value of 3.0–3.5 and a following increase until a prebrightening value of about 4.5, the modeled $E_{g\downarrow}$ shows stronger variations (decrease) than the modeled SD (e.g., from the panel in row 1 and column 2 of Figure 7, for T_L moving from 3.0 to 4.5, SD is expected to decrease about one third less than $E_{g\downarrow}$). The same behavior can be observed starting from the prebrightening value (about 4.5) and decreasing T_L until an ending value of 3.0–3.5. Also, in this case there is a stronger variation (increase) of the modeled $E_{g\downarrow}$ with respect to the modeled SD (e.g., from the panel in row 4 and column 2 of Figure 7, for T_L moving from 4.5 to 3.0, SD is expected to increase about one third less than $E_{g\downarrow}$). The modeled variations are in agreement with the observed clear-sky series (Figures 3, 5, and 6).

In summer (July), the modeled $E_{g\downarrow}$ variations are only slightly stronger than the modeled SD ones both when T_L increases between a predimming equal to about 4.5 and a prebrightening equal to 5.5–6.0 and when it decreases to an ending value of about 4 (Figure 7) as obtained for the observed $E_{g\downarrow}$ and SD records (Figures 3, 5, and 6). It is also interesting to underline that the higher T_L values in the north could explain the only case for which the observed $E_{g\downarrow}$ does not have stronger variations than SD during the dimming period (considering, e.g., T_L predimming and prebrightening values equal to about 5.5 and 6.5).

In autumn (October), from the modeled results, $E_{g\downarrow}$ is expected to have higher variations than SD both when T_L increases between a predimming value of 3.0–3.5 to a prebrightening value of about 4.5 and when it

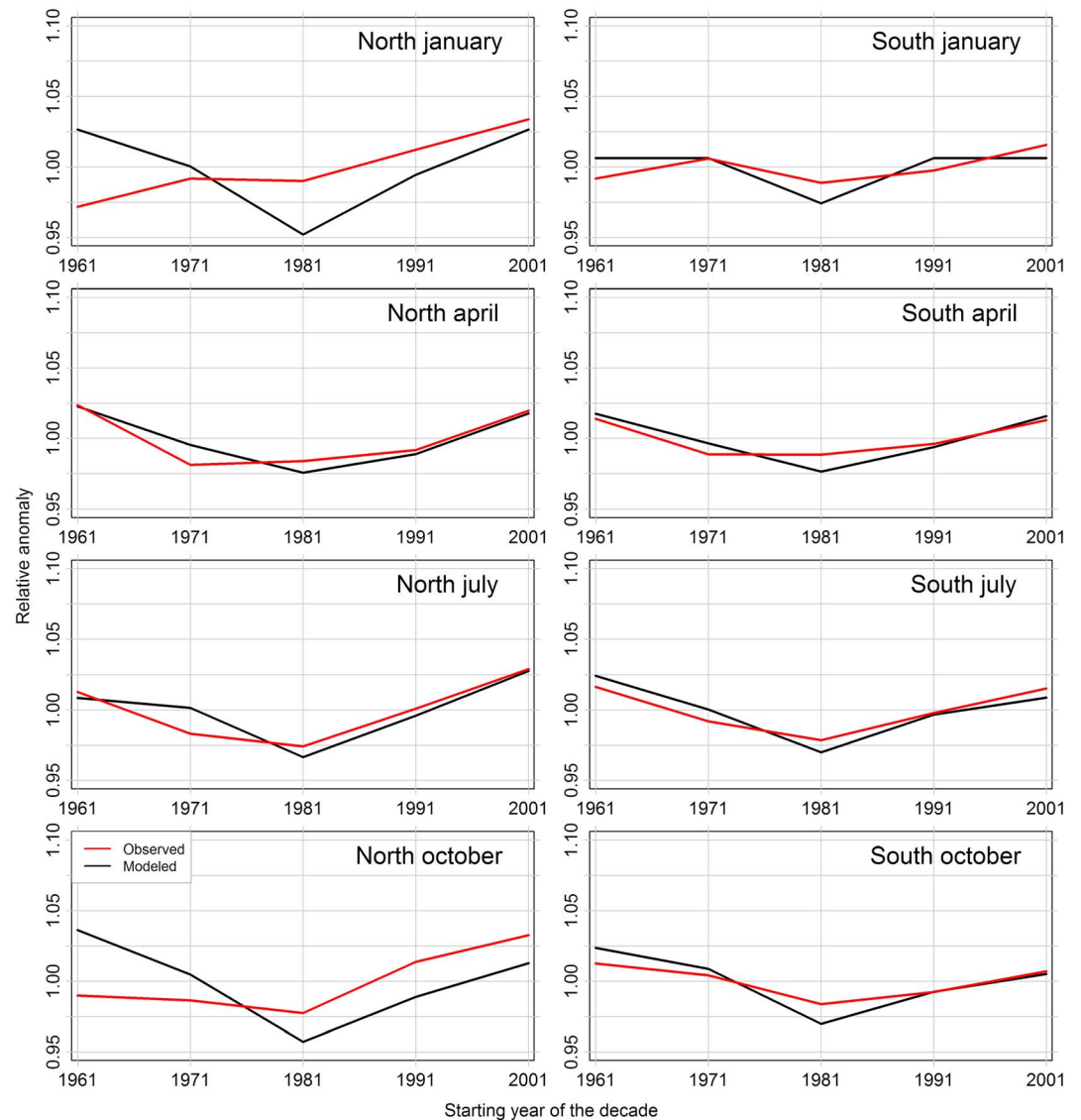


Figure 9. Northern (left side) and southern (right side) Italy modeled (black line) and observed clear-sky (red line) SD relative anomalies calculated for each decade of the 1961–2010 period. The x axis show the starting year of the considered decade. Results refer to the central month of each season.

decreases to an ending value of 3.0–3.5 (Figure 7). This agrees with the results reported for clear-sky conditions, even though simulated values do not explain the weak decrease of the observed SD (see Figure 5) in the dimming period especially in the north.

A similar behavior is observed in winter (January): the modeled $E_{g\downarrow}$ is expected to have higher variations than the corresponding SD both when T_L increases from a predimmed of 2.5–3.0 to a prebrightening of 3.5–4.0 and when it decreases to an ending value of 2.5–3.0 (Figure 7). In this case for southern Italy the simulated impacts of the atmospheric turbidity evolution on $E_{g\downarrow}$ and SD are in reasonable agreement with the observations (Figures 3, 5, and 6), whereas for northern Italy, during the dimming period, relevant discrepancies are evident.

Overall, the results above show that the SD and $E_{g\downarrow}$ sensitivity to T_L variations strongly depends on the T_L starting value. In order to highlight this behavior, we investigated the relative decrease of modeled SD and $E_{g\downarrow}$ corresponding to an increase of T_L of one unit for any integer T_L in the range 2–7 (Figure 8). The results highlight that for T_L lower than 4, SD is less sensitive than $E_{g\downarrow}$ (to changes in T_L) while for T_L values higher than 6 the behavior is opposite. The intersection between the SD and $E_{g\downarrow}$ curves is around T_L equal to 5–6 with the

only exception of winter in the north where it is around T_L equal to 4–5. Moreover, the difference in sensitivity of the two variables is particularly strong for low T_L values especially in January (winter) and October (autumn). Winter is therefore the season in which the largest differences in the SD and $E_{g\downarrow}$ trends are expected because it has both the lowest T_L values and the highest difference in the sensitivity of SD and $E_{g\downarrow}$ to T_L variations. For the other seasons and for their typical T_L values, the sensitivity of SD and $E_{g\downarrow}$ to T_L changes is expected to be more similar (Figures 7 and 8) even though in most cases $E_{g\downarrow}$ is more sensitive than SD, with the only exception of summer for T_L around 6 where a stronger SD sensitivity is expected.

In order to further investigate the agreement between modeled and observed clear-sky SD trends, we estimated northern and southern Italy T_L values for each decade of the 1961–2010 period. Then, we applied equation (1) to get the corresponding decadal SD values. Finally, we calculated the relative anomalies (for both modeled and observed values) with respect to the averages over these five decades, and we compared them. The results (Figure 9) highlight an excellent agreement between the modeled and the observed SD trends in spring (April) and in summer (July), as already observed in the comparison between observed clear-sky trends (Figure 5) and modeled variations (Figure 7). In the other two seasons, in southern Italy the agreement is rather good, while in the north it is reasonable during the brightening period but very poor during the dimming period. The discrepancy is stronger in winter than in autumn.

6. Discussion and Conclusions

Two homogenized data sets of sunshine duration (SD) [Manara *et al.*, 2015] and global radiation ($E_{g\downarrow}$) [Manara *et al.*, 2016a] records covering the Italian territory were used to investigate to what extent these two variables agree with respect to their temporal evolution, under both all-sky and clear-sky conditions. The analysis has been performed considering annual and seasonal regional series for northern and southern Italy over the 1959–2013 period.

The results highlight that the agreement between the decadal variability and long-term trends of SD and $E_{g\downarrow}$ depends on the considered region, season, and period. Overall, under all-sky conditions, the SD records show a shorter and less intense decrease during the dimming period with respect to the $E_{g\downarrow}$ ones, while the agreement is better if the subsequent period is considered, where both variables show an increasing tendency. This behavior is reflected in the $E_{g\downarrow}/SD$ ratio records that show a significant decrease until the mid-1980s, which is more pronounced in winter and autumn (especially due to a lack of a negative SD trend), while in the subsequent period the ratio records do not show any significant trends. Considering only clear days, the ratio records show again a decrease until the mid-1980s and a weaker increase in the subsequent period with the exception of summer in northern Italy where the $E_{g\downarrow}/SD$ ratio record does not show any significant trend.

In order to investigate whether the differences in the clear-sky SD and $E_{g\downarrow}$ trends are due to a different sensitivity to atmospheric turbidity changes, we applied a model to estimate how large the SD and $E_{g\downarrow}$ relative variations are when atmospheric turbidity (expressed by means of the turbidity Linke factor— T_L) increases or decreases. Then, we considered a realistic temporal pattern for T_L , and we checked if the differences in the observed SD and $E_{g\downarrow}$ trends could be explained on the basis of their different sensitivity to the T_L variations. It is interesting to underline that the results reported in Figures 7 and 8 can be used also if different temporal patterns of T_L are considered for the same area.

The sensitivity analysis showed that the clear-sky SD and $E_{g\downarrow}$ sensitivity to T_L variations strongly depends on the absolute value of T_L . Specifically, for low T_L ($T_L < 3$), $E_{g\downarrow}$ is much more sensitive than SD, while for high T_L ($T_L > 6$), SD is slightly more sensitive than $E_{g\downarrow}$. This result has to be kept in mind when SD is used as a proxy variable to investigate multidecadal variations of $E_{g\downarrow}$. A further problem may be linked to the position of stations without an optimal sky-view factor either at sunrise or at sunset or in both circumstances. When the reduction of the sky-view factor is large, this problem can completely hide the response of clear-sky SD to T_L variations. In this case, direct radiation reaches the Campbell-Stokes sunshine recorder only when its value is already above the instrumental threshold. Therefore, the clear-sky SD simply corresponds to the time interval in which the sun is visible from the considered station, independently from T_L and so SD is not sensitive to T_L changes. Our stations are generally located in plain or coastal areas and have a good sky-view factor. We can however not exclude that the modeled SD variations may be slightly

overestimated by a nonoptimal sky-view factor for few stations. This problem is more relevant in winter when the T_L values are low.

The comparison between the modeled and the observed SD relative trends highlights a very good agreement in southern Italy. In northern Italy, good agreement is found in the brightening period, whereas in the dimming period only in spring and summer. In winter and autumn, the differences in the observed trends of SD and $E_{g\downarrow}$ cannot be explained by their different sensitivity to T_L variations. We do not have a conclusive explanation for this issue. A possible factor could be a decrease of relative humidity, which was not captured by the method we used to estimate the temporal variation of T_L . This method is in fact based on $E_{g\downarrow}$ records and focuses therefore on the central hours of the day, which are those that most contribute to global radiation. A reduction of relative humidity in the hours of SD sensitivity to T_L (sunrise and sunset) in the 1960s and 1970s could therefore be a physical process which would explain what we observe. Such mechanism could, e.g., be driven by an increase of the urbanization close to some of the station sites. High relative humidity may also alter the radiative properties of the particles suspended in the atmosphere increasing their radiative forcing [Kotchenruther et al., 1999; Xia et al., 2007]. This is particularly important during the winter season in the north where fog episodes are rather frequent. As far as those episodes are concerned, Giulianelli et al. [2014] report a significant decrease of fog episodes at a Po Plain site (San Pietro Capo Fiume) during the brightening period. Unfortunately, their data do not cover the dimming period too. Nevertheless, it is worth noting that in other Mediterranean regions, a widespread decrease in relative humidity has been reported during the dimming period [Vicente-Serrano et al., 2014].

All the problems related to the different sensitivity of clear-sky SD and $E_{g\downarrow}$ to T_L do not limit the use of SD as a good proxy to highlight cloudiness induced $E_{g\downarrow}$ variations as shown in other studies [Sanchez-Lorenzo and Wild, 2012; Wang, 2014]. SD has however to be considered with great attention in studying the multidecadal evolution of $E_{g\downarrow}$ where the changes in aerosol concentration play a relevant role, especially if T_L is low and if it shows significant temporal changes. A more detailed understanding of the unexpected trends in the winter (and autumn) northern Italy SD clear-sky records in the dimming period and of the differences observed under all-sky conditions calls for further research including the study of other variables such as relative humidity, visibility, and cloudiness.

References

- Angstrom, A. (1924), Solar and terrestrial radiation, *Q. J. R. Meteorol. Soc.*, *50*(210), 121–126, doi:10.1002/qj.49705021008.
- Antón, M., J. M. Vaquero, and A. J. P. Aparicio (2014), The controversial early brightening in the first half of 20th century: A contribution from pyrhemometer measurements in Madrid (Spain), *Global Planet. Change*, *115*, 71–75, doi:10.1016/j.gloplacha.2014.01.013.
- Antón, M., R. Román, A. Sanchez-Lorenzo, J. Calbó, and J. M. Vaquero (2017), Variability analysis of the reconstructed daily global solar radiation under all-sky and cloud-free conditions in Madrid during the period 1887–1950, *Atmos. Res.*, *191*, 94–100, doi:10.1016/j.atmosres.2017.03.013.
- Bartók, B. (2016), Aerosol radiative effects under clear skies over Europe and their changes in the period of 2001–2012, *Int. J. Climatol.*, doi:10.1002/joc.4821.
- Baumgartner, T. (1979), Die Schwellenintensität des Sonnenscheinautographen Campbell-Stokes an wolkenlosen Tagen, *Arbeitsberichte der Schweizerischen Meteorol. Zentralanstalt*, *84*.
- Baynard, T., R. M. Garland, A. R. Ravishankara, M. A. Tolbert, and E. R. Lovejoy (2006), Key factors influencing the relative humidity dependence of aerosol light scattering, *Geophys. Res. Lett.*, *33*, L06813, doi:10.1029/2005GL024898.
- Bider, M. (1958), Über die Genauigkeit der Registrierungen des Sonnenscheinautographen Campbell-Stokes, *Arch. Meteorol. Geophys. Bioklimatol. B*, *9*(2), 199–230, doi:10.1007/BF02242909.
- Brazdil, R., A. A. Flocas, and H. S. Sahsamanoglou (1994), Fluctuation of sunshine duration in central and south-eastern Europe, *Int. J. Climatol.*, *14*(9), 1017–1034, doi:10.1002/joc.3370140907.
- Brunetti, M., M. Maugeri, T. Nanni, I. Auer, R. Böhm, and W. Schöner (2006), Precipitation variability and changes in the Greater Alpine Region over the 1800–2003 period, *J. Geophys. Res.*, *111*, D11107, doi:10.1029/2005JD006674.
- Che, H. Z., G. Y. Shi, X. Y. Zhang, R. Arimoto, J. Q. Zhao, L. Xu, B. Wang, and Z. H. Chen (2005), Analysis of 40 years of solar radiation data from China, 1961–2000, *Geophys. Res. Lett.*, *32*, L06803, doi:10.1029/2004GL022322.
- Chiachio, M., and M. Wild (2010), Influence of NAO and clouds on long-term seasonal variations of surface solar radiation in Europe, *J. Geophys. Res.*, *115*, D00D22, doi:10.1029/2009JD012182.
- Cutforth, H. W., and D. Judiesch (2007), Long-term changes to incoming solar energy on the Canadian Prairie, *Agric. For. Meteorol.*, *145*, 167–175, doi:10.1016/j.agrformet.2007.04.011.
- Dutton, E. G., A. Farhadi, R. S. Stone, C. N. Long, and D. W. Nelson (2004), Long-term variations in the occurrence and effective solar transmission of clouds as determined from surface-based total irradiance observations, *J. Geophys. Res.*, *109*, D03204, doi:10.1029/2003JD003568.
- Dutton, E. G., D. W. Nelson, R. S. Stone, D. Longenecker, G. Carbaugh, J. M. Harris, and J. Wendell (2006), Decadal variations in surface solar irradiance as observed in a globally remote network, *J. Geophys. Res.*, *111*, D19101, doi:10.1029/2005JD006901.
- Enriquez-Alonso, A., A. Sanchez-Lorenzo, J. Calbó, J. A. González, and J. R. Norris (2016), Cloud cover climatologies in the Mediterranean obtained from satellites, surface observations, reanalyses, and CMIP5 simulations: Validation and future scenarios, *Clim. Dyn.*, *47*(1–2), 249–269, doi:10.1007/s00382-015-2834-4.

Acknowledgments

The homogenized and gap-filled station records used in this paper are those presented in [Manara et al., 2015] and [Manara et al., 2016a] for sunshine duration and global radiation, respectively. They obtained raw data by different sources (web sites and contact persons are provided for data access). The data were recovered by CREA (“Consiglio per la ricerca in agricoltura e l’analisi dell’economia agraria”), and they are available at <http://cma.entecra.it/homePage.htm> since 1994 for sunshine duration and global radiation. The sunshine duration data of the previous years have to be requested at CREA. Sunshine duration, global radiation, and total cloud cover data from the Italian Air Force (“Servizio dell’Aeronautica Militare Italiana” refer to: <http://clima.meteoam.it/istruzioni.php> for data access) have been received in the frame of an agreement between Italian Air Force and the Italian National Research Council. Luca Lombroso and Maurizio Ratti provided the sunshine duration series of the Geophysical Observatory of Modena, and the sunshine duration series of the Meteorological Observatory of Pontremoli (“Osservatorio meteorologico Marsili”). The Trieste records of sunshine duration and global radiation are available online at <http://www.meteo.units.it/>. The Varese data for sunshine duration are available on request at “Centro Geofisico Prealpino-Società Astronomica G.V. Schiaparelli”, <http://www.astrogeo.va.it/>. The Swiss solar radiation data have been obtained from the Swiss Federal Office for Meteorology and Climatology (MeteoSwiss), and they are available at <http://www.meteosvizzera.admin.ch/> and <https://gate.meteoswiss.ch/ida-web/login.do>. Arturo Sanchez-Lorenzo was supported by a postdoctoral fellowship JCI-2012-12508 and projects CGL2014-55976-R and CGL2014-52135-C3-1-R financed by the Spanish Ministry of Economy and Competitiveness. Dimming/brightening research at ETH Zurich is supported by the Swiss National Science Foundation grants 200021 135395 and 200020 159938. We also kindly acknowledge Ruth Loewenstein for her help in improving the English.

- Giulianelli, L., S. Gilardoni, L. Tarozzi, M. Rinaldi, S. Decesari, C. Carbone, M. C. Facchini, and S. Fuzzi (2014), Fog occurrence and chemical composition in the Po valley over the last twenty years, *Atmos. Environ.*, *98*, 394–401, doi:10.1016/j.atmosenv.2014.08.080.
- Grenier, J. C., A. De La Casinière, and T. Cabot (1995), Atmospheric turbidity analyzed by means of standardized Linke's turbidity factor, *J. Appl. Meteorol.*, *34*, 1449–1458.
- Hansen, J., M. Sato, and R. Ruedy (1997), Radiative forcing and climate response, *J. Geophys. Res.*, *102*, 6831–6864, doi:10.1029/96JD03436.
- Hartmann, D. L., V. Ramanathan, A. Berroir, and G. E. Hunt (1986), Earth radiation budget data and climate research, *Rev. Geophys.*, *24*, 439–468, doi:10.1029/RG024i002p00439.
- Horseman, A., A. R. MacKenzie, and R. Timmis (2008), Using bright sunshine at low-elevation angles to compile an historical record of the effect of aerosol on incoming solar radiation, *Atmos. Environ.*, *42*(33), 7600–7610, doi:10.1016/j.atmosenv.2008.06.033.
- Iqbal, M. (1983), *An Introduction to Solar Radiation*, chap. 1, pp. 1–28, Academic Press, Don Mills, Ontario, Canada.
- Jacovides, C. P. (1997), Model comparison for the calculation of Linke's turbidity factor, *Int. J. Climatol.*, *17*, 551–563, doi:10.1002/(SICI)1097-0088(199704)17:5<551::AID-JOC137>3.0.CO;2-C.
- Kerr, A., and R. Tabony (2004), Comparison of sunshine recorded by Campbell–Stokes and automatic sensors, *Weather*, *59*(4), 90–95.
- Kopp, G., and J. L. Lean (2011), A new, lower value of total solar irradiance: Evidence and climate significance, *Geophys. Res. Lett.*, *38*, L01706, doi:10.1029/2010GL045777.
- Kotchenruther, R. A., P. V. Hobbs, and D. A. Hegg (1999), Humidification factors for atmospheric aerosols off the mid-Atlantic coast of the United States, *J. Geophys. Res.*, *104*, 2239–2251, doi:10.1029/98JD01751.
- Lelieveld, J., et al. (2002), Global air pollution crossroads over the Mediterranean, *Science*, *298*(5594), 794–799, doi:10.1126/science.1075457.
- Liang, F., and X. A. Xia (2005), Long-term trends in solar radiation and the associated climatic factors over China for 1961–2000, *Ann. Geophys.*, *23*(7), 2425–2432, doi:10.5194/angeo-23-2425-2005.
- Liepert, B., and I. Tegen (2002), Multidecadal solar radiation trends in the United States and Germany and direct tropospheric aerosol forcing, *J. Geophys. Res.*, *107*(D12), 4153, doi:10.1029/2001JD000760.
- Liepert, B., P. Fabian, and H. Grassl (1994), Solar radiation in Germany—observed trends and an assessment of their causes. Part I: Regional approach, *Contrib. Atmos. Phys.*, *67*(1), 15–29.
- Liepert, B. G., and G. J. Kukla (1997), Decline in global solar radiation with increased horizontal visibility in Germany between 1964 and 1990, *J. Clim.*, *10*(9), 2391–2401, doi:10.1175/1520-0442(1997)010<2391:DIGSRW>2.0.CO;2.
- Lohmann, S., C. Schillings, B. Mayer, and R. Meyer (2006), Long-term variability of solar direct and global radiation derived from ISCCP data and comparison with reanalysis data, *Sol. Energy*, *80*(11), 1390–1401, doi:10.1016/j.solener.2006.03.004.
- Manara, V., M. C. Beltrano, M. Brunetti, M. Maugeri, A. Sanchez-Lorenzo, C. Simolo, and S. Sorrenti (2015), Sunshine duration variability and trends in Italy from homogenized instrumental time series (1936–2013), *J. Geophys. Res. Atmos.*, *120*, 3622–3641, doi:10.1002/2014JD022560.
- Manara, V., M. Brunetti, A. Celozzi, M. Maugeri, A. Sanchez-Lorenzo, and M. Wild (2016a), Detection of dimming/brightening in Italy from homogenized all-sky and clear-sky surface solar radiation records and underlying causes (1959–2013), *Atmos. Chem. Phys.*, *16*(17), 11,145–11,161, doi:10.5194/acp-16-11145-2016.
- Manara, V., M. Brunetti, M. Maugeri, A. Sanchez-Lorenzo, and M. Wild (2016b), Homogenization of a surface solar radiation dataset over Italy, in *Radiation Processes in the Atmosphere and Ocean (IRS 2016)—AIP Conference Proceeding*, pp. 090004–1–090004-4.
- Manara, V., M. Brunetti, and M. Maugeri (2016c), Reconstructing sunshine duration and solar radiation long-term evolution for Italy: A challenge for quality control and homogenization procedures, in *14th IMEKO TC10 Workshop Technical Diagnostics—New Perspectives in Measurements, Tools and Techniques for System's Reliability, Maintainability and Safety*, pp. 13–18, IMEKO, Milan, Italy.
- Matuszko, D. (2012), Influence of cloudiness on sunshine duration, *Int. J. Climatol.*, *32*(10), 1527–1536, doi:10.1002/joc.2370.
- Maugeri, M., Z. Bagnati, M. Brunetti, and T. Nanni (2001), Trends in Italian total cloud amount, 1951–1996, *Geophys. Res. Lett.*, *28*, 4551–4554, doi:10.1029/2001GL013754.
- Nabat, P., S. Somot, M. Mallet, A. Sanchez-Lorenzo, and M. Wild (2014), Contribution of anthropogenic sulfate aerosols to the changing Euro-Mediterranean climate since 1980, *Geophys. Res. Lett.*, *41*, 5605–5611, doi:10.1002/2014GL060798.
- Norris, J. R., and M. Wild (2007), Trends in aerosol radiative effects over Europe inferred from observed cloud cover, solar “dimming,” and solar “brightening”, *J. Geophys. Res.*, *112*, D08214, doi:10.1029/2006JD007794.
- Oguz, E., M. D. Kaya, and Y. Nuhoglu (2003), Interaction between air pollution and meteorological parameters in Erzurum, Turkey, *Int. J. Environ. Pollut.*, *19*(3), 292–300, doi:10.1504/IJEP.2003.003312.
- Ohmura, A., and H. Gilgen (1993), Re-evaluation of the global energy balance, in *Interactions Between Global Climate Subsystems: The Legacy of Hann*, *Geophys. Monogr. Ser.*, vol. 75, edited by G. A. McBean and M. Hantel, pp. 93–110, AGU, Washington, D. C.
- Painter, H. E. (1981), The performance of a Campbell–Stokes sunshine recorder compared with a simultaneous record of the normal incidence irradiance, *Meteorol. Mag.*, *110*(1305), 102–109.
- Power, H. C. (2003), Trends in solar radiation over Germany and an assessment of the role of aerosols and sunshine duration, *Theor. Appl. Climatol.*, *76*, 47–63, doi:10.1007/s00704-003-0005-8.
- Prescot, J. A. (1940), Evaporation from a water surface in relation to solar radiation, *Trans. R. Soc. South Aust.*, *64*, 114–118.
- Qian, Y., W. Wang, L. R. Leung, and D. P. Kaiser (2007), Variability of solar radiation under cloud-free skies in China: The role of aerosols, *Geophys. Res. Lett.*, *34*, L12804, doi:10.1029/2006GL028800.
- Ramanathan, V., P. J. Crutzen, J. T. Kiehl, and D. Rosenfeld (2001), Aerosols, climate, and the hydrological cycle, *Science*, *294*(5549), 2119–2124, doi:10.1126/science.1064034.
- Rigollier, C., O. Bauer, and L. Wald (2000), On the clear sky model of the ESRA—European Solar Radiation Atlas with respect to the Heliosat method, *Sol. Energy*, *68*(1), 33–48, doi:10.1016/S0038-092X(99)00055-9.
- Román, R., J. Bilbao, and A. de Miguel (2014), Reconstruction of six decades of daily total solar shortwave irradiation in the Iberian Peninsula using sunshine duration records, *Atmos. Environ.*, *99*, 41–50, doi:10.1016/j.atmosenv.2014.09.052.
- Sanchez-Lorenzo, A., and M. Wild (2012), Decadal variations in estimated surface solar radiation over Switzerland since the late 19th century, *Atmos. Chem. Phys.*, *12*(18), 8635–8644, doi:10.5194/acp-12-8635-2012.
- Sanchez-Lorenzo, A., J. Calbó, M. Brunetti, and C. Deser (2009), Dimming/brightening over the Iberian Peninsula: Trends in sunshine duration and cloud cover and their relations with atmospheric circulation, *J. Geophys. Res.*, *114*, D00D09, doi:10.1029/2008JD011394.
- Sanchez-Lorenzo, A., J. Calbó, M. Wild, C. Azolina-Molina, and A. Sanchez-Romero (2013), New insights into the history of the Campbell–Stokes sunshine recorder, *Weather*, *68*(12), 327–331, doi:10.1002/wea.2130.
- Sanchez-Lorenzo, A., M. Wild, M. Brunetti, J. A. Guijarro, M. Z. Hakuba, J. Calbó, S. Mystakidis, and B. Bartok (2015), Reassessment and update of long-term trends in downward surface shortwave radiation over Europe (1939–2012), *J. Geophys. Res. Atmos.*, *120*, 9555–9569, doi:10.1002/2015JD023321.

- Sanchez-Romero, A., A. Sanchez-Lorenzo, J. Calbó, J. A. González, and C. Azorin-Molina (2014), The signal of aerosol-induced changes in sunshine duration records: A review of the evidence, *J. Geophys. Res. Atmos.*, *119*, 4657–4673, doi:10.1002/2013JD021393.
- Sanchez-Romero, A., J. A. Gonzalez, J. Calbo, and A. Sanchez-Lorenzo (2015), Using digital image processing to characterize the Campbell-Stokes sunshine recorder and to derive high-temporal resolution direct solar irradiance, *Atmos. Meas. Tech.*, *8*, 183–194, doi:10.5194/amt-8-183-2015.
- Sen, P. K. (1968), Estimates of the regression coefficient based on Kendall's tau, *J. Am. Stat. Assoc.*, *63*(324), 1379–1389, doi:10.1080/01621459.1968.10480934.
- Soni, V. K., G. Pandithurai, and D. S. Pai (2012), Evaluation of long-term changes of solar radiation in India, *Int. J. Climatol.*, *32*(4), 540–551, doi:10.1002/joc.2294.
- Stanhill, G. (1983), The distribution of global solar radiation over the land surfaces of the Earth, *Sol. Energy*, *31*(1), 95–104.
- Stanhill, G. (2003), Through a glass brightly: Some new light on the Campbell-Stokes sunshine recorder, *Weather*, *58*(1), 3–11.
- Stanhill, G. (2005), Global dimming: A new aspect of climate change, *Weather*, *60*(1), 11–14, doi:10.1256/wea.210.03.
- Stanhill, G., and O. Achiman (2016), Early global radiation measurements: A review, *Int. J. Climatol.*, doi:10.1002/joc.4826.
- Stanhill, G., and S. Cohen (2001), Global dimming: A review of the evidence for a widespread and significant reduction in global radiation with discussion of its probable causes and possible agricultural consequences, *Agric. For. Meteorol.*, *107*(4), 255–278, doi:10.1016/S0168-1923(00)00241-0.
- Stanhill, G., and S. Cohen (2005), Solar radiation changes in the United States during the twentieth century: Evidence from sunshine duration measurements, *Am. Meteorol. Soc.*, *18*(10), 1503–1512.
- Stanhill, G., and J. D. Kalma (1995), Solar dimming and urban heating at hong kong, *Int. J. Climatol.*, *15*(8), 933–941.
- Tang, I. N. (1996), Chemical and size effects of hygroscopic aerosols on light scattering coefficients, *J. Geophys. Res.*, *101*, 19,245–19,250, doi:10.1029/96JD03003.
- Tang, W., K. Yang, J. He, and J. Qin (2010), Quality control and estimation of global solar radiation in China, *Sol. Energy*, *84*(3), 466–475, doi:10.1016/j.solener.2010.01.006.
- Tang, W. J., K. Yang, J. Qin, C. C. K. Cheng, and J. He (2011), Solar radiation trend across China in recent decades: A revisit with quality-controlled data, *Atmos. Chem. Phys.*, *11*(1), 393–406, doi:10.5194/acp-11-393-2011.
- Theil, H. (1950), A rank-invariant method of linear and polynomial regression analysis, in *Proceedings of the Royal Academy of Sciences*, pp. 386–392, North Holland Publ. Co., Amsterdam.
- Vestreng, V., G. Myhre, H. Fagerli, S. Reis, and L. Tarrasón (2007), Twenty-five years of continuous sulphur dioxide emission reduction in Europe, *Atmos. Chem. Phys.*, *7*(13), 3663–3681, doi:10.5194/acp-7-3663-2007.
- Vicente-Serrano, S. M., C. Azorin-Molina, A. Sanchez-Lorenzo, E. Morán-Tejeda, J. Lorenzo-Lacruz, J. Revuelto, J. I. López-Moreno, and F. Espejo (2014), Temporal evolution of surface humidity in Spain: Recent trends and possible physical mechanisms, *Clim. Dyn.*, *42*(9), 2655–2674, doi:10.1007/s00382-013-1885-7.
- Wang, K. (2014), Measurement biases explain discrepancies between the observed and simulated decadal variability of surface incident solar radiation, *Sci. Rep.*, *4*(1), 6144, doi:10.1038/srep06144.
- Wang, K., Q. Ma, Z. Li, and J. Wang (2015), Decadal variability of surface incident solar radiation over China: Observations, satellite retrievals, and reanalyses, *J. Geophys. Res. Atmos.*, *120*, 6500–6514, doi:10.1002/2015JD023420.
- Wang, K. C., R. E. Dickinson, M. Wild, and S. Liang (2012), Atmospheric impacts on climatic variability of surface incident solar radiation, *Atmos. Chem. Phys.*, *12*(20), 9581–9592, doi:10.5194/acp-12-9581-2012.
- Wild, M. (2009), Global dimming and brightening: A review, *J. Geophys. Res.*, *114*, D00D16, doi:10.1029/2008JD011470.
- Wild, M. (2012), Enlightening global dimming and brightening, *Bull. Am. Meteorol. Soc.*, *93*, 27–37, doi:10.1175/BAMS-D-11-00074.1.
- Wild, M. (2016), Decadal changes in radiative fluxes at land and ocean surfaces and their relevance for global warming, *Wiley Interdiscip. Rev. Clim. Change*, *7*(1), 91–107, doi:10.1002/wcc.372.
- Wild, M., H. Gilgen, A. Roesch, A. Ohmura, C. N. Long, E. G. Dutton, B. Forgan, A. Kallis, V. Russak, and A. Tsvetkov (2005), From dimming to brightening: Decadal changes in solar radiation at Earth's surface, *Science*, *308*(5723), 847–850, doi:10.1126/science.1103215.
- Wild, M., B. Trüssel, A. Ohmura, C. N. Long, G. König-Langlo, E. G. Dutton, and A. Tsvetkov (2009), Global dimming and brightening: An update beyond 2000, *J. Geophys. Res.*, *114*, D00D13, doi:10.1029/2008JD011382.
- World Meteorological Organization (1969), Guide to Meteorological instrument and observing practices, 3rd ed., Secretariat of the World Meteorol. Organ., pp. 31–35, Geneva, Switzerland.
- World Meteorological Organization (2008a), Measurement of radiation, in *Guide to Meteorological Instruments and Methods of Observation*, pp. 1.7 1–1.7 42, World Meteorol. Organ., Geneva, Switzerland.
- World Meteorological Organization (2008b), Measurement of sunshine duration, in *Guide to Meteorological Instruments and Methods of Observation*, pp. 1.81–1.811, World Meteorol. Organ., Geneva, Switzerland.
- Xia, X. (2010), Spatiotemporal changes in sunshine duration and cloud amount as well as their relationship in China during 1954–2005, *J. Geophys. Res.*, *115*, D00K06, doi:10.1029/2009JD012879.
- Xia, X. (2012), Significant decreasing cloud cover during 1954–2005 due to more clear-sky days and less overcast days in China and its relation to aerosol, *Ann. Geophys.*, *30*(3), 573–582, doi:10.5194/angeo-30-573-2012.
- Xia, X., Z. Li, B. Holben, P. Wang, T. Eck, H. Chen, M. Cribb, and Y. Zhao (2007), Aerosol optical properties and radiative effects in the Yangtze Delta region of China, *J. Geophys. Res.*, *112*, D22S12, doi:10.1029/2007JD008859.
- You, Q., S. Kang, W. A. Flugel, A. Sanchez-Lorenzo, Y. Yan, J. Huang, and M. V. Javier (2010), From brightening to dimming in sunshine duration over the eastern and central Tibetan Plateau (1961–2005), *Theor. Appl. Climatol.*, *101*(6), 445–457, doi:10.1007/s00704-009-0231-9.
- Zhang, Y. L., B. Q. Qin, and W. M. Chen (2004), Analysis of 40 year records of solar radiation data in Shanghai, Nanjing and Hangzhou in eastern China, *Theor. Appl. Climatol.*, *78*, 217–227, doi:10.1007/s00704-003-0030-7.